Exploration and Mining Geology, Vol. 17, Nos. 1–2, p. 101–130, 2008

0964-1823/00 $17.00 + .00

Geologic, Geochemical, and Geochronological Constraints on the Genesis of Gold Mineralization at Poplar Mountain, Western New Brunswick, Canada

G. CHI[1,†], S. WATTERS[2,*], W.J. DAVIS[3], P. NI[4], S. CASTONGUAY[5], AND D. HOY[6]

(Received September 15, 2003; accepted July 30, 2006)

Abstract — The Poplar Mountain gold occurrence in western New Brunswick is hosted in the Poplar Mountain volcanic complex (PMVC), which is located along the southern segment of the regional Woodstock fault zone. The PMVC consists of three principal units including, in ascending order, a porphyritic felsic volcanic unit, a volcaniclastic unit, and a mafic volcanic unit. U–Pb dating of zircon indicates that the age of the volcanic rocks is younger than 459 ± 3 Ma, and $^{40}Ar/^{39}Ar$ dating of mineralization-associated sericite indicates that the age of mineralization is 411 ± 3.7 Ma. Gold-mineralized zones occur in all the lithologic units but mainly in the porphyritic felsic volcanic unit. Gold zones are not controlled by individual faults but are characterized by high-density brittle fracturing, thin carbonate-quartz veining, and intensive ankerite–sericite alteration, superimposed on an earlier chlorite–calcite–quartz alteration. Gold is associated with arsenopyrite, which mostly occurs as disseminations in the host rocks, and to a lesser extent with quartz–carbonate–sericite veins and quartz-cemented breccias.

Geochemical data indicate that mineralization-associated alteration is characterized by enrichment of K, Rb, Cs, Ca, Sr, Ba, As, Sb, W, C, and S. Fluid inclusion data indicate that the mineralizing fluids are composed of H_2O, salts, and CO_2 with variable amounts of N_2 and CH_4; salinities range from 2.3 to 10.6 eq. wt.% NaCl, but mainly from 2.3 to 5.6 eq. wt.% NaCl, and homogenization temperatures lie mainly between 220° and 270°C. Fluid pressures at the site of mineralization are estimated to have been 770 to 1200 bars, corresponding to a depth of 2.9 to 4.6 km at lithostatic pressure. The $\delta^{18}O_{SMOW}$ and $\delta^{13}C_{PDB}$ values of mineralization-related ankerite range from +14.5‰ to +16.5‰, and –6.8‰ to –8.3‰, respectively. The $\delta^{18}O$ values of the ore-forming fluids are estimated to be 6.4‰ to 8.3‰ at a temperature of 250°C. These carbon and oxygen isotope data fall in the field of magmatic fluids and in part the field of metamorphic fluids.

Considering the geological setting of the region, abundant granitic intrusions, the similarity between the age of mineralization (411 ± 3.7 Ma) and the nearby Pokiok batholith (402–415 Ma), and the enrichment of granophile elements in mineralization-related alteration, the ore-forming fluids were probably derived from a granitic intrusion underneath the PMVC. These fluids were focused along structures related to the Woodstock fault. The Poplar Mountain gold occurrence might be compared to some granitic intrusion-related gold systems based on the geochemical data presented herein.

Key Words: Gold deposits, intrusion-related gold systems, Poplar Mountain, Ar–Ar dating, fluid inclusions, CO_2, isocon.

Sommaire — L'indice aurifère de Poplar Mountain dans l'ouest du Nouveau Brunswick est contenu dans le complexe volcanique de Poplar Mountain (CVPM), lequel est situé le long du segment sud de la zone de faille régionale de Woodstock. Les trois unités principales du CVPM sont, de la base au sommet, une unité volcanique felsique porphyrique, une unité volcaniclastique et une unité volcanique mafique. La datation U–Pb de zircons indique que les roches volcaniques sont plus jeunes que 459 ± 3 Ma, et la datation par la méthode $^{40}Ar/^{39}Ar$ de séricite associée à la minéralisation assigne à la minéralisation un age de 411 ± 3.7 Ma. Bien que les zones minéralisées en or soient présentes dans toutes les unités lithologiques, on les retrouve surtout dans l'unité felsique porphyrique. Les zones aurifères ne sont pas contrôlées par des failles individuelles mais sont caractérisées par une grande densité de fractures cassantes, de minces veines de quartz-carbonate, et par une altération en ankérite–séricite intense qui se superpose à une altération antérieure en chlorite–calcite–quartz. L'or est associé à l'arsénopyrite, laquelle est principalement présente à l'état de disséminations dans la roche hôte, et à un moindre degré avec des veines de quartz–carbonate–séricite et des brèches à ciment de quartz.

Les données de géochimie indiquent que l'altération associée à la minéralisation est caractérisée par un enrichissement en K, Rb, Cs, Ca, Sr, Ba, As, Sb, W, C, et S. Les inclusions fluides indiquent que les fluides minéralisants, étaient composés de H_2O, de sels, et de CO_2 accompagnés de quantités variables de N_2 et de CH_4; les valeurs de salinité varient entre 2.3 et 10.6 équivalent poids % NaCl, mais se situent principalement entre 2.3 à 5.6 équivalent poids % NaCl, et les températures d'homogénéisation sont comprises entre 220° et 270° C. La pression des fluides au site de mise en place de la minéralisation est estimée entre 770 et 1200 bars, ce qui correspond à une profondeur comprise entre 2.9 et 4.6 km dans un contexte de pression lithostatique. Les valeurs de $\delta^{18}O_{SMOW}$ et de $\delta^{13}C_{PDB}$ de l'ankérite associées à la minéralisation sont respectivement comprises entre +14.5 ‰ et +16.5‰ et entre –6.8‰ et –8.3‰. La valeur du $\delta^{18}O$ du fluide minéralisant est estimée entre 6.4 ‰ et 8.3‰ à une température de 250°C.

Étant donné le contexte géologique de la région, l'abondance des intrusions granitiques, la similitude entre l'âge de la minéralisation (411 ±3.7 Ma) et celui du batholite avoisinant de Pokiok (402–415 Ma), et l'enrichissement en éléments granophiles notées dans l'altération associée à la minéralisation, les fluides minéralisants sont probablement dérivés d'une intrusion granitique sous le CVPM. Ces fluides ont été concentrés le long des structures associées à la faille Woodstock. Les données géochimiques présentées ici permettent d'établir une comparaison entre l'indice aurifère de Poplar Mountain et certains systèmes aurifères associés aux intrusions granitiques.

---

[1]Department of Geology, University of Regina, 3737 Wascana Parkway, Regina, Saskatchewan, S4S 0A2.
[2]New Brunswick Department of Natural Resources, Geological Surveys Branch, 207 Picadilly Road, Sussex, New Brunswick, E4E 5L2.
[3]Geological Survey of Canada, Continental Geoscience Division, 601 Booth Street, Ottawa, Ontario, K1A 0E8.
[4]Department of Earth Sciences, Nanjing University, Nanjing, 210093 P. R. China.
[5]Geological Survey of Canada, Québec Division, 490 rue de la Couronne, Québec, Québec, G1K 9A9.
[6]Freewest Resources Canada Inc., 855 Field Street, Thunder Bay, Ontario, P7B 6B6.
[*]*Present address:* 3262 Hwy. 121, Apohaqui, New Brunswick, E5P 1B1.
[†]*Corresponding author.* E-mail: guoxiang.chi@uregina.ca

Introduction

The Poplar Mountain gold occurrence, located in western New Brunswick (Fig. 1), is one of the most important gold discoveries in New Brunswick in recent years (McLeod et al., 2008). The mineralization is hosted in a volcanic complex known as the Poplar Mountain volcanic complex (PMVC), which is close to the Woodstock fault, a major regional structure, and is 8 km from the surface contact of the Pokiok batholith (Fig. 1). The host rocks and location with respect to structures and intrusions have led to three different hypotheses regarding the origin of the mineralization. First, because the mineralization is mainly hosted in porphyritic volcanic or subvolcanic rocks, it has been classified as porphyry type (McLeod and McCutcheon, 2000), or a type lying between the outer zone of a porphyry system and an epithermal system (Chi and Watters, 2002). Second, Freewest Resources Canada Inc. (unpub. report, 1999) emphasized features indicating a shallow crustal environment and the structural control associated with the Woodstock fault. The spatial association of regional gold mineralization with the Woodstock fault has been noted previously (Ruitenberg et al., 1990). A third possibility is that the mineralization at Poplar Mountain is related to unexposed granitic intrusions. This hypothesis warrants examination considering the proximity of Poplar Mountain to the Pokiok batholith, and the overall similarities between some gold occurrences in the region and intrusion-related gold systems (Lang et al., 2000; Lang and Baker, 2001) or gold deposits related to reduced granitic intrusions (Thompson and Newberry, 2000; Chi, 2002; McLeod et al., 2008). A better understanding of the genesis of gold mineralization at Poplar Mountain is important for further exploration in the region, because different genetic models will lead to different exploration strategies. This study was undertaken in order to elucidate the structural, stratigraphic, and temporal controls on mineralization and related hydrothermal alteration, and the temperature, pressure, and origin of the ore-forming fluids at Poplar Mountain.

Regional Geological Setting

The study area is part of the northern Appalachian orogen, which consists of NE-trending Lower Paleozoic tectonic zones overlain by Middle Paleozoic basins and Upper Paleozoic successor basins (Williams, 1995). The Lower Paleozoic tectonic zones in New Brunswick comprise, from northwest to southeast, the Dunnage, Gander, and Avalon zones (Fig. 1). The Poplar Mountain area lies near the southwestern end of the Miramichi terrane (Fig. 1), in rocks assigned to the Gander zone. The Miramichi terrane is bounded by the Woodstock fault to the northwest and by the Meductic fault to the southeast. To the northwest of the Woodstock fault lies the Late Ordovician to Late Silurian Matapedia basin, whereas to the southeast of the Meductic fault is the Late Silurian to Early Devonian Canterbury basin (Fig. 1).

The Miramichi terrane consists of the Woodstock Group and the overlying Meductic Group (Fyffe, 2001). The Woodstock Group (Cambrian to Early Ordovician) is com-

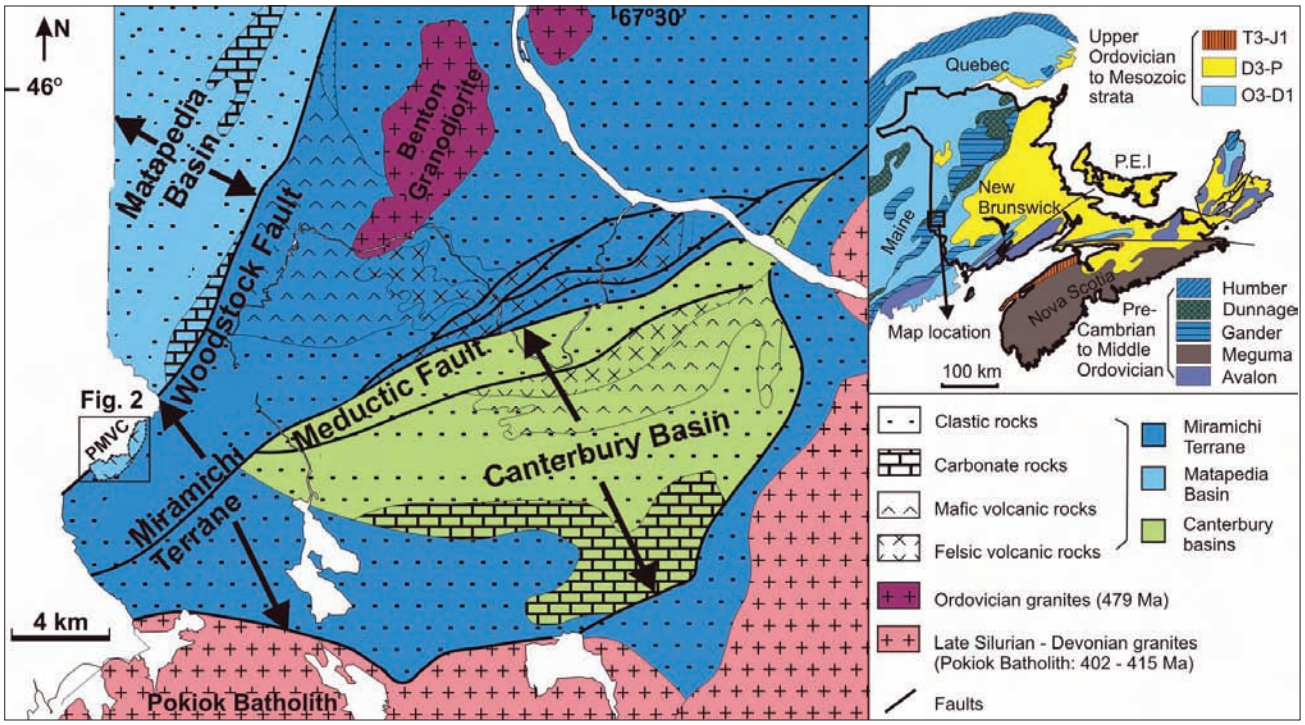

Fig. 1. Regional geological map of part of southwestern New Brunswick, showing the location of the Poplar Mountain volcanic complex (PMVC) relative to other tectonostratigraphic units (modified from NBDNRE, 2000). Colors indicate different ages/units, and patterns indicate different lithologies.

posed of interbedded quartz wacke and shale of the Baskahegan Lake Formation, and silty mudstone and shale in the overlying Bright Eye Brook Formation. The Meductic Group (Early Ordovician to Middle Ordovician) is divided into four formations, which in ascending order are: Porten Road Formation, Eel River Formation, Oak Mountain Formation, and Belle Lake Formation. The first three formations contain felsic, intermediate, and mafic volcanic rocks, respectively, whereas the Belle Lake Formation consists of feldspathic wacke and shale.

The Matapedia basin consists of the Carys Mills Formation (Late Ordovician to Early Silurian) and the overlying Smyrna Mills Formation (Early to Late Silurian; Bourque et al., 1995). Abundant volcanic and volcaniclastic rocks occur in the Ellen Wood Ridge Formation in Maine, which might be correlated with the upper part of the Smyrna Mills Formation (Hopeck, 2001).

The Canterbury basin is composed of the Perham Group (Late Silurian) and the overlying Tobique Group (Early Devonian). The Perham Group contains marine clastic rocks and minor carbonate rocks, whereas the Tobique Group consists of shallow marine clastic and volcanic rocks (Rast et al., 1980).

The strata of the Miramichi terrane were subject to deformation beginning in Middle to Late Ordovician, whereas the strata of the Matapedia and Canterbury basins were deformed during the Mid-Devonian Acadian orogeny. The strata of the Miramichi terrane and the Late Silurian strata of the Fredericton basin located further to the southeast were intruded by the Pokiok batholith (Fig. 1), isotopic ages for which range from 402 to 415 Ma (Bevier and Whalen, 1990).

In addition to Poplar Mountain, there are several gold occurrences in western New Brunswick. A few of these lie to the northeast along the Woodstock fault (outside Fig. 1), e.g., the quartz-carbonate veins at Britton mine and Bull Creek (Ruitenberg et al., 1990). The Connell Mountain porphyry Cu-Au deposit occurs within the Miramichi terrane, to the northeast of the map area of Fig. 1 (Ruitenberg et al., 1990). Gold mineralization has been noted (M. McLeod, pers. commun., 2003) at the Gravel Hill base metal sulfide deposit, which is developed in a Lower Devonian felsic volcanic dome complex of the Tobique Group (Ruitenberg, 1994) about 50 km northeast of Poplar Mountain. A gold-arsenopyrite breccia occurrence is located near the northwestern margin of the Pokiok batholith (D. Lentz, pers. commun., 2003), whereas the Lake George W-Mo-Sb-Au deposit, formerly the most important Sb producer in North America, lies to the southeast of the batholith (Yang et al., 2002).

Analytical Methods

In addition to field investigation and conventional microscopic petrographic examination, this study includes major and trace element analysis, U–Pb and $^{40}Ar/^{39}Ar$ isotopic dating, fluid inclusion analysis, and C and O isotopic analysis of carbonates. The major elements and a few trace elements were analyzed by ICP-AES at Institut National de Recherche Scientifique–Eau, Terre, et Environnement (INRS-ETE) in Quebec City. Most trace elements were analyzed by ICP-MS at the same institute. Some trace elements were analyzed by INAA at XRAL Laboratories; C was analyzed by LECO at the same laboratory. The method of analysis for each element is shown in Table 1.

U–Pb and $^{40}Ar/^{39}Ar$ isotopic analyses were carried out at the Geological Survey of Canada (GSC) laboratories in Ottawa, Ontario. U–Pb ion probe data were acquired using the GSC Sensitive High-Resolution Ion Microprobe (SHRIMP II). The samples for $^{40}Ar/^{39}Ar$ isotopic analysis were irradiated at the research reactor of McMaster University, Ontario, and the laser $^{40}Ar/^{39}Ar$ step-heating analysis was carried out at the GSC (Ottawa). A detailed description of the isotopic analytical methods and data treatment is provided in Appendix A.

Fluid inclusions were studied by microthermometry and laser Raman microspectroscopy. Fluid-inclusion microthermometry was carried out using USGS-style heating-freezing stages made by Fluid Inc. at the Geological Survey of Canada, Quebec Division, and the Department of Geology, University of Regina. The precision of temperature measurements was ±0.2°C at low temperatures and ±1°C at high temperatures. Laser Raman analyses were carried out at the State Key Laboratory for Mineral Deposit Research, Nanjing University, China, using a Renishaw RM2000 laser Raman microscope (excitation laser wavelength = 514 nm, laser energy = 5 mW), and using silicon as the standard (520 cm^{-1} Raman shift). The Raman spectrum collecting time was 2 minutes for each fluid inclusion.

The C and O isotopes of carbonates were analyzed at the Geological Survey of Canada, Delta Lab, in Quebec City. Carbon dioxide liberated from carbonates was analyzed with a VG-SIRA 12 mass spectrometer. The accuracy of analysis (Vienna PDB standard) was ±0.2‰ for $\delta^{18}O$ and ±0.1‰ for $\delta^{13}C$, and the analytical precision was better than ±0.1‰ for both $\delta^{13}C$ and $\delta^{18}O$.

The Poplar Mountain Volcanic Complex

The volcanic rocks hosting the gold mineralization at Poplar Mountain are part of the Poplar Mountain volcanic complex (PMVC). The PMVC has an ellipsoidal shape of about 4.5 km long and 1.5 km wide, and is located along the Woodstock fault (Fig. 1) at the southwest end of the Miramichi terrane. The sedimentary rocks of the Belle Lake Formation and the Matapedia basin lie to the east and west of the PMVC respectively, whereas volcanic rocks of the Meductic Group lie to the northeast, and sedimentary and volcanic rocks of the Canterbury basin are situated further to the east (Fig. 1). The age of the PMVC is problematic because no direct contacts with these other strata have been exposed (Chi and Watters, 2002).

Lithological Units

The PMVC can be divided into three principal units comprising porphyritic felsic volcanic rocks, volcaniclastic rocks, and mafic volcanic rocks, respectively (Watters and Chi, 2002; Fig. 2). The characteristics of these units are

Table 1. Major and Trace Element Compositions of Volcanic Rocks and Quartz-Carbonate Veins from Poplar Mountain and Vicinity

	Sample	Description	Locality (core interval, m)	SiO_2 (%)[a]	TiO_2 (%)[a]	Al_2O_2 (%)[a]	$Fe_2O_3^T$ (%)[a]
Mafic volcanic rocks	GC01-133	Basalt with spherulitic texture/least altered	GR99-8 (62.2–62.35)	45.45	0.59	15.97	12.15
	GC01-135	Basalt with spherulitic texture/least altered	GR99-8 (65.6–65.75)	45.36	0.61	16.43	11.26
	GC01-136	Basalt/least altered	GR99-9 (82.9–83.0)	50.37	2.34	13.78	12.08
	GC01-138	Basalt/least altered	GR99-9 (66.2–66.3)	50.59	2.20	13.41	12.09
	GC01-127-1	Basalt/altered (buff)	GR99-8 (51.7–51.75)	36.59	0.46	13.34	8.89
	GC01-127-2	Basalt/altered (buff to light green)	GR99-8 (51.75–51.8)	41.71	0.56	14.01	9.84
	GC01-127-3	Basalt/altered (light to median green)	GR99-8 (51.8–51.85)	44.45	0.59	14.72	11.12
	GC01-73	Mafic dike intruding felsic volcanic rock	GR99-10 (53–53.1)	53.57	3.46	15.91	5.45
Volcaniclastic rocks	GC01-55-1	Plagioclase-rich/least altered	Trench-5	51.81	0.59	19.65	6.54
	GC01-55-2	Finer-grained/least altered	Trench-5	73.64	0.59	10.64	3.79
	GC01-140	Least altered	GR99-6 (49.5–49.8)	59.76	0.56	16.00	8.95
	01SW15	Plagioclase-rich/least altered	GR99-2 (10.8–11.0)	45.87	0.84	20.16	11.40
	97SW-134-1	Fragment/least altered	Angular float	59.98	0.65	16.99	4.83
	97SW-134-2	(0.5 frag + 0.5 matrix)/least altered	Angular float	63.76	0.49	16.02	4.88
	GC01-129	Intercalated in basalt (with bedding)	GR99-8 (35.2–35.45)	71.01	0.12	9.97	3.81
	01SW42	Intercalated in basalt (mineralized)	GR99-8	59.27	0.24	13.69	4.39
	GC01-134	Intercalated in basalt (mineralized)	GR99-8 (40.75–40.90)	64.50	0.05	6.51	13.88
Felsic volcanic rocks	01SW46-1	Least altered	GR99-3 (58.4–58.6)	63.28	0.49	15.13	4.12
	GC01-40	Least altered	Trench-5	67.79	0.46	13.57	3.21
	GC01-79	Least altered	GR99-10 (95.6–95.7)	68.51	0.51	14.41	4.69
	01SW11-2	Least altered	GR99-10 (98–98.1)	69.53	0.45	12.71	3.19
	GC01-78	Brecciated fragment/least altered	GR99-10 (99.5–99.75)	70.28	0.47	12.84	4.37
	01SW10	Brecciated fragment/least altered	GR99-10 (98.2–98.4)	68.23	0.47	12.85	4.11
	01SW11-1	Brecciated fragment/least altered	GR99-10 (98–98.1)	66.10	0.46	14.03	4.07
	GC01-78	Brecciated fragment/least altered	GR99-10 (99.5–99.75)	70.28	0.47	12.84	4.37
	01SW10	Brecciated fragment/least altered	GR99-10 (98.2–98.4)	68.23	0.47	12.85	4.11
	01SW11-1	Brecciated fragment/least altered	GR99-10 (98–98.1)	66.10	0.46	14.03	4.07
	GC01-74	Altered (adjacent to ser + carb vein)	GR99-10 (26.5–26.65)	70.69	0.46	12.61	2.82
	01SW46-2	Altered (adjacent to ser + carb vein)	GR99-3 (58.4–58.6)	64.84	0.49	14.76	3.62
	01SW44	Altered	GR99-9	62.17	0.47	11.24	4.19
	GC01-80	Altered (buff)	GR99-10 (84.05–84.25)	66.34	0.46	13.56	3.49
	GC01-81	Altered (buff)	GR99-10 (106.2–106.35)	66.08	0.50	14.59	3.98
	GC01-77	Altered (buff)	GR99-10 (166.6–166.7)	56.19	0.64	18.25	4.53
	GC01-67	Altered, sheared, mineralized	GR99-5 (73.5–73.7)	60.99	0.50	14.70	4.90
	GC01-69	Brecciated and mineralized	GR99-5 (42.75–42.9)	68.26	0.53	13.71	3.51
	01SW39	Altered and mineralized	GR99-6	71.48	0.36	10.51	3.41
	01SW32	Brecciated and mineralized	GR99-6	68.66	0.47	13.67	3.64
	GC01-47	Altered and mineralized	Trench-5	60.21	0.49	14.47	5.10
	GC01-61	Altered and mineralized	GR99-2 (96.1–96.3)	64.16	0.47	13.56	4.30
	GC01-62	Altered and mineralized	GR99-2 (94.6–94.74)	51.14	0.46	15.01	5.49
	GC01-63	Altered and mineralized	GR99-2 (93.2–93.44)	65.00	0.45	13.89	3.35
	GC01-64	Altered (buff-taupe)	GR99-2 (88.17–88.25)	65.47	0.42	12.75	3.02
	GC01-65	Altered (buff with green phenocrysts)	GR99-2 (85.3–85.42)	66.26	0.48	14.36	3.04
	GC01-59	Altered and mineralized	GR99-2 (102.87–102.96)	64.67	0.47	13.81	4.44
	GC01-60	Altered and mineralized	GR99-2 (98.9–99.1)	63.39	0.47	13.87	4.20
	GC01-71	Altered with pyrite	GR99-10 (17.7–17.82)	66.07	0.42	12.76	3.68
	97SW46	Altered and mineralized	Near Trench-3	59.69	0.44	13.41	5.22
Veins and breccia	GC01-44	Qz vein (44 cm wide)	Trench-5	96.75	0.01	0.45	0.36
	GC01-45	Early black quartz vein	Trench-5	96.90	0.00	0.33	0.33
	GC01-125-1	Felsic volcanic breccia (adjacent to cockscomb qz)	Trench-2	91.81	0.07	2.88	1.34
	GC01-125-2	Cockscomb quartz	Trench-2	96.33	0.00	0.49	0.05
	GC01-123	Felsic volcanic breccia + quartz matrix/mineralized	Trench-1	75.93	0.16	7.31	5.19
	76618	Quartz vein with sphalerite and Sb/along E−W fault	Trench-2	86.28	0.09	2.95	1.49
	76608	Quartz vein	Trench-3	95.72	0.01	0.43	0.80
	76650	Quartz vein	Trench-4	94.27	0.01	0.48	1.75
Devonian volcanic & intrusive rocks	GC01-32	Mafic volcanic/Dorrington Hill Fmn	Highway 122	52.85	1.64	15.70	9.27
	GC01-38	Mafic volcanic/Dorrington Hill Fmn	Highway 122	52.63	1.87	14.99	10.56
	GC01-29	Dow porphyry	Highway 122	68.87	0.55	14.04	3.51

Table 1. (Continued)

MnO (%)[a]	MgO (%)[a]	CaO (%)[a]	Na_2O (%)[a]	K_2O (%)[a]	P_2O_5 (%)[a]	LOI (%)[a]	Total (%)[a]	S (%)[a]	C (%)[b]	Co (ppm)[c]	Cr (ppm)[c]	Sc (ppm)[c]	V (ppm)[a]	Ba (ppm)[a]	Sr (ppm)[a]	Rb (ppm)[d]
0.18	7.70	10.43	0.92	0.01	0.10	5.60	99.24	0.03	0.07	49	90	46	347.2	31.0	202.8	0.6
0.19	6.66	11.80	1.14	0.01	0.10	5.70	99.39	0.04	0.22	43	104	46	349.3	24.4	226.8	0.8
0.20	5.08	6.47	2.97	0.07	0.36	4.57	98.56	0.09	0.23	43	27	28	272.0	627.1	293.9	1.3
0.19	4.39	7.10	2.81	0.07	0.38	5.51	99.03	0.10	0.56	33	24	25	238.0	177.4	716.7	1.7
0.16	5.00	10.78	0.34	1.92	0.08	20.60	98.67	0.39	5.16	31	170	31	280.8	288.1	256.7	53.0
0.17	5.79	7.26	0.87	1.40	0.09	15.50	97.43	0.12	3.42	32	111	36	314.3	250.9	168.1	43.0
0.19	6.51	6.73	1.15	0.88	0.09	12.91	99.48	0.03	2.41	35	154	38	320.7	190.5	125.6	24.9
0.07	0.99	4.72	5.54	1.52	1.19	7.12	100.10	0.35	1.67	16	11	30	338.2	360.9	304.8	33.3
0.05	4.28	3.92	1.61	3.21	0.20	7.38	99.39	0.01	0.79	12	<10	21	92.2	509.1	267.8	74.1
0.03	1.98	1.09	2.52	1.11	0.13	2.56	98.17	0.01	0.18	10	11	17	72.5	212.7	185.1	25.5
0.09	1.77	0.63	5.21	1.69	0.18	2.92	98.46	0.62	0.10	30	<10	28	101.6	325.8	87.3	39.2
0.07	4.19	4.04	2.78	3.08	0.29	7.22	100.09	0.02	0.86	14	26	30	118.0	464.5	131.3	66.2
0.04	1.84	2.03	7.18	0.50	0.22	3.55	97.92	0.01	0.58	<5	<10	20	69.3	159.8	429.8	12.2
0.05	1.89	1.96	4.88	0.94	0.17	4.68	99.84	0.02	0.94	7	12	17	65.0	317.1	283.8	21.2
0.05	2.51	0.89	0.30	2.25	<0.03	6.44	97.43	0.01	1.40	6	<10	4	14.7	355.8	66.7	60.8
0.08	2.39	4.38	0.22	3.48	0.03	9.70	98.98	0.82	1.97	<5	<10	8	87.6	477.8	198.6	98.1
0.16	2.31	0.62	0.17	0.35	<0.03	9.56	99.56	1.41	1.99	14	15	2	17.2	49.0	23.2	9.3
0.08	0.79	2.74	4.43	3.85	0.18	3.01	98.29	0.01	0.55	9	<10	17	60.9	904.7	214.6	55.0
0.07	0.42	3.80	3.37	3.05	0.16	2.28	98.39	0.02	0.35	8	10	14	56.5	786.4	488.0	50.4
0.05	1.01	1.15	4.25	2.38	0.18	2.51	99.79	0.02	0.26	9	275	17	59.5	448.0	145.2	63.4
0.04	0.67	2.03	3.92	1.84	0.17	4.48	99.15	0.03	1.01	<5	23	9	55.1	371.3	187.6	30.6
0.05	0.93	1.61	4.24	2.22	0.17	2.25	99.56	0.02	0.27	<5	10	12	41.8	602.0	199.4	46.6
0.05	0.97	2.15	3.88	2.42	0.17	4.72	100.13	0.01	1.08	<5	15	14	55.3	421.2	200.4	63.3
0.04	0.86	1.27	3.67	2.33	0.16	4.22	97.31	0.02	0.83	<5	<10	15	58.6	333.4	144.7	60.6
0.05	0.93	3.25	3.39	2.37	0.17	4.06	100.67	0.23	0.89	7	18	14	70.1	472.6	140.6	50.8
0.05	0.97	2.92	3.31	4.28	0.19	3.55	99.14	0.08	0.58	10	12	14	63.1	1147.3	237.9	78.3
0.04	0.86	4.91	2.74	1.56	0.06	8.75	98.99	0.43	2.16	12	<10	25	228.7	184.8	338.7	37.6
0.05	0.48	3.44	3.38	2.56	0.17	5.14	99.47	0.20	1.19	6	113	13	59.0	459.9	307.1	50.8
0.09	0.83	1.99	2.81	2.63	0.18	5.46	99.16	0.04	1.07	<5	31	16	63.1	480.3	184.7	49.5
0.11	1.96	3.24	1.84	3.03	0.20	8.93	98.77	0.05	1.77	9	90	19	77.5	573.9	352.1	71.6
0.13	0.48	3.44	3.38	2.56	0.17	5.14	99.47	0.20	1.19	6	113	13	59.0	459.9	307.1	50.8
0.12	0.67	1.99	2.81	2.63	0.18	5.46	99.16	0.04	1.07	<5	31	16	63.1	480.3	184.7	49.5
0.05	1.67	3.24	1.84	3.03	0.20	8.93	98.77	0.05	1.77	9	90	19	77.5	573.9	352.1	71.6
0.09	0.95	3.59	0.56	3.46	0.16	7.72	99.34	0.82	1.32	<5	78	16	62.7	604.2	181.2	69.1
0.05	0.89	2.64	2.08	2.82	0.19	5.50	101.23	0.54	1.00	5	131	16	61.5	478.3	146.7	62.4
0.05	0.79	3.17	0.66	2.89	0.14	5.45	99.31	0.33	1.12	8	156	11	48.3	385.1	84.3	68.0
0.06	0.64	2.15	0.81	3.49	0.18	5.20	100.37	0.70	0.70	7	132	14	62.9	553.2	104.0	75.7
0.11	1.22	2.96	1.36	3.08	0.17	7.64	96.95	0.05	1.68	5	49	17	61.3	545.5	135.9	56.1
0.06	1.15	2.43	2.34	2.92	0.15	5.72	98.90	0.83	0.97	<5	108	16	58.6	352.3	154.4	75.6
0.15	1.53	6.04	0.12	4.12	0.19	10.21	96.87	0.96	2.10	7	128	22	69.9	551.7	354.0	81.4
0.07	0.82	2.88	2.38	2.92	0.17	5.30	98.57	0.72	0.94	8	178	15	57.8	463.0	223.1	67.9
0.08	0.35	3.50	4.57	1.57	0.16	5.00	97.77	0.77	1.00	11	171	13	53.0	336.5	228.5	42.4
0.04	0.98	2.07	3.51	2.88	0.18	4.58	98.56	0.08	0.92	<5	181	14	57.6	434.8	149.5	85.0
0.04	0.69	1.63	3.53	2.34	0.16	4.69	98.46	0.97	0.62	<5	169	21	62.9	498.5	180.0	50.9
0.06	0.79	2.77	3.09	2.93	0.17	5.31	98.54	0.86	0.91	<5	194	16	60.9	461.3	204.0	74.5
0.06	0.47	3.16	3.04	2.53	0.15	4.90	97.98	0.63	0.95	8	230	17	55.6	429.0	192.9	63.9
0.09	1.15	3.37	0.21	3.36	0.14	8.04	97.32	0.94	1.47	<5	21	17	59.1	625.9	140.1	77.6
0.00	0.03	0.10	0.02	0.11	<0.03	0.31	98.19	0.01	0.34	<5	277	<1	<10.2	20.0	4.7	2.8
0.01	0.01	0.03	0.01	0.09	<0.03	0.10	97.86	0.01	0.03	<5	279	2	<10.3	22.1	2.4	2.4
0.00	0.04	0.04	0.04	0.74	<0.03	0.86	97.99	0.03	0.03	<5	199	4	12.7	148.0	16.6	14.4
0.00	0.01	0.02	0.03	0.02	<0.03	0.25	97.21	<0.0053	<0.01	<5	<10	<1	<10.6	21.1	3.8	0.9
0.01	0.14	0.36	0.12	1.62	0.10	4.73	98.08	1.08	0.15	<5	230	6	29.4	323.5	30.6	37.4
0.05	0.17	0.99	0.04	0.69	0.07	2.44	97.00	0.30	0.40	<5	<10	3	10.7	126.9	31.3	15.2
0.00	0.03	0.05	0.02	0.10	<0.03	0.81	98.50	0.34	0.03	<5	<10	<1	<10.6	23.5	5.2	2.8
<0.00053	0.01	0.03	0.02	0.11	<0.03	1.81	99.97	0.47	0.02	<5	72	<1	<10.6	44.3	2.6	2.6
0.15	5.77	5.15	5.59	0.75	0.37	2.03	99.39	0.01	0.06	33	120	33	214.8	187.8	232.3	21.2
0.23	4.23	5.44	5.71	0.73	0.79	1.37	98.69	0.01	0.07	18	43	37	145.3	308.7	287.9	20.5
0.07	1.05	2.29	5.09	1.80	0.14	1.71	99.24	0.01	0.22	10	60	10	58.5	339.5	298.3	85.8

Table 1. (Continued)

	Sample	Cs (ppm)[d]	Y (ppm)[d]	Zr (ppm)[d]	Hf (ppm)[d]	Nb (ppm)[d]	Ta (ppm)[d]	Th (ppm)[d]	U (ppm)[d]	La (ppm)[d]	Ce (ppm)[d]	Pr (ppm)[d]	Nd (ppm)[d]	Sm (ppm)[d]	Eu (ppm)[d]	Gd (ppm)[d]
Mafic volcanic rocks	GC01-133	.6	9.5	25.6	.7	2.3	.1	1.3	.4	6.1	13.5	1.7	7.7	1.8	.6	1.8
	GC01-135	.6	10.3	27.5	.8	2.3	.1	1.3	.4	6.8	14.8	1.8	8.3	1.9	.6	1.9
	GC01-136	1.0	42.6	319.7	7.3	37.6	2.5	3.7	1.1	32.2	72.1	8.9	39.1	8.4	2.4	8.3
	GC01-138	1.7	46.2	383.9	8.3	42.5	2.9	4.2	1.4	34.9	80.0	9.8	42.2	9.1	2.8	8.8
	GC01-127-1	13.0	8.1	21.6	.6	1.9	.1	1.1	.3	5.5	12.4	1.6	6.8	1.6	.5	1.6
	GC01-127-2	10.4	9.4	25.5	.7	2.2	.1	1.3	.4	6.1	13.6	1.7	7.5	1.8	.6	1.8
	GC01-127-3	8.0	10.1	25.5	.7	2.3	.1	1.2	.4	6.4	13.9	1.8	7.7	1.8	.7	1.8
	GC01-73	2.4	156.9	229.0	5.2	29.5	2.0	2.5	4.8	54.2	108.3	13.1	57.4	12.7	2.8	14.3
Volcaniclastic rocks	GC01-55-1	8.3	45.7	197.7	4.7	12.0	.8	11.0	2.4	62.3	91.5	11.8	47.6	8.5	2.2	7.8
	GC01-55-2	3.2	25.4	98.2	2.5	10.9	.5	5.6	1.5	33.9	58.5	7.3	28.1	5.0	1.1	4.4
	GC01-140	1.6	21.2	114.6	3.0	8.4	.6	7.8	1.3	12.2	31.7	4.1	18.6	4.6	.9	4.1
	01SW15	6.4	25.0	216.6	6.1	14.8	1.1	14.8	3.2	36.4	71.7	8.1	34.2	6.6	1.6	5.7
	97SW-134-1	1.6	23.3	157.7	4.7	8.9	.9	11.6	.8	38.1	78.7	8.7	36.3	6.7	1.6	5.4
	97SW-134-2	4.1	27.4	137.5	3.4	10.3	.6	8.3	.6	32.5	67.6	7.7	31.7	6.0	1.4	5.2
	GC01-129	4.9	14.5	104.3	2.8	7.6	.7	8.7	1.9	28.9	55.6	6.0	22.6	4.1	.9	3.3
	01SW42	5.9	17.4	145.2	3.4	12.4	.7	8.6	1.9	16.2	36.3	4.2	16.5	3.5	.8	3.1
	GC01-134	2.1	5.9	28.3	.8	3.4	.2	1.6	.7	11.0	19.2	2.0	7.7	1.4	.3	1.2
Felsic volcanic rocks	01SW46-1	.8	24.4	136.9	3.5	9.2	.6	8.5	2.4	28.4	61.3	6.8	27.9	5.2	1.2	4.3
	GC01-40	.9	22.4	131.4	3.3	9.0	.6	7.9	2.0	28.6	58.3	6.7	26.9	5.0	1.1	4.4
	GC01-79	2.3	21.1	135.8	3.6	9.3	.6	8.5	2.0	26.5	56.6	6.7	27.2	5.3	1.2	4.5
	01SW11-2	3.0	16.0	113.3	3.3	7.9	.6	7.6	2.0	24.2	51.1	5.9	23.9	4.5	1.1	3.9
	GC01-78	2.8	18.4	112.8	3.3	7.9	.6	7.9	1.7	21.9	49.4	5.7	23.4	4.6	1.0	4.0
	01SW10	3.8	19.2	121.7	3.3	8.3	.6	8.0	1.7	22.9	50.7	5.9	23.7	4.6	1.0	3.9
	01SW11-1	3.2	19.8	126.6	3.5	8.7	.6	8.5	1.9	26.9	58.3	6.5	25.4	4.8	1.1	4.1
	GC01-74	1.6	17.6	117.9	3.1	7.8	.6	7.3	1.9	16.4	39.3	4.8	20.0	4.1	.9	3.5
	01SW46-2	1.9	28.1	137.2	3.5	9.1	.6	8.4	2.9	28.8	59.8	6.9	28.0	5.4	1.0	4.9
	01SW44	2.3	13.6	33.2	.9	3.0	.2	1.8	.5	9.1	18.2	2.1	9.0	1.8	.5	1.9
	GC01-80	2.1	21.0	128.1	3.3	8.4	.6	8.1	1.9	27.9	57.8	6.5	26.6	5.0	1.1	4.4
	GC01-81	6.4	22.0	130.2	3.4	8.9	.6	8.3	2.2	28.5	60.5	7.0	27.9	5.2	1.1	4.6
	GC01-77	7.9	33.0	198.6	5.4	13.5	.9	12.7	4.3	39.9	85.4	9.8	38.8	7.5	1.5	6.4
	GC01-67	3.8	21.3	142.0	3.4	9.5	.6	8.0	2.0	26.6	57.6	6.6	25.9	5.0	1.1	4.3
	GC01-69	3.0	32.0	135.1	3.4	9.6	.6	8.2	1.9	25.4	58.5	6.9	27.1	5.4	1.3	4.6
	01SW39	2.3	16.6	98.9	2.5	6.9	.5	6.0	1.7	18.7	41.2	4.7	18.7	3.7	.9	3.2
	01SW32	3.4	24.8	131.9	3.3	9.3	.6	7.9	2.6	24.5	53.3	6.2	24.4	4.7	1.0	4.1
	GC01-47	4.9	20.8	139.2	3.5	9.5	.6	8.3	2.0	25.9	58.3	6.6	26.0	5.0	1.1	4.2
	GC01-61	3.0	20.6	139.1	3.4	9.6	.6	7.9	1.9	22.5	50.9	6.1	23.9	4.7	1.1	4.0
	GC01-62	2.2	43.3	134.9	3.6	8.9	.7	9.0	2.1	29.8	68.3	7.9	32.4	7.0	1.8	7.3
	GC01-63	1.9	21.9	136.1	3.3	9.2	.6	7.8	1.9	25.7	56.4	6.5	25.5	5.0	1.1	4.3
	GC01-64	2.4	21.8	134.0	3.3	9.2	.6	7.7	2.4	25.4	55.6	6.3	24.8	4.8	1.1	4.1
	GC01-65	2.7	22.1	138.8	3.4	9.7	.6	8.0	2.1	25.4	54.7	6.3	24.6	4.7	1.1	4.0
	GC01-59	1.5	22.3	144.4	3.5	10.0	.6	8.3	1.9	27.4	60.0	6.8	26.7	5.1	1.1	4.3
	GC01-60	2.7	20.3	142.0	3.5	9.7	.6	8.2	1.9	26.4	57.3	6.6	26.0	4.9	1.1	4.1
	GC01-71	2.3	19.8	128.1	3.1	9.0	.5	7.4	1.8	24.3	51.2	5.8	23.1	4.4	1.0	3.7
	97SW46	5.4	21.0	140.2	3.3	9.7	.6	7.9	1.9	26.4	57.0	6.4	25.0	4.6	1.0	4.0
Veins and breccia	GC01-44	.1	.5	5.6	.1	.4	0.0	.2	.1	.7	1.5	.2	.7	.1	0.0	.1
	GC01-45	.1	1.4	3.1	0.0	.2	<0.005	.1	4.5	.3	.5	.1	.3	.1	0.0	.1
	GC01-125-1	.5	3.6	19.1	.5	1.6	.1	1.2	.3	6.3	12.4	1.4	5.4	1.0	.2	.8
	GC01-125-2	.2	.1	1.1	0.0	.1	<0.005	.1	<0.02	.2	.5	.1	.2	0.0	0.0	0.0
	GC01-123	1.8	8.7	47.2	1.2	3.4	.2	3.0	.9	11.9	26.4	3.1	12.2	2.3	.6	2.0
	76618	.7	8.0	27.9	.7	2.0	.1	1.6	.5	6.5	14.5	1.7	7.0	1.7	.5	1.7
	76608	.1	.9	4.3	.1	.3	0.0	.2	.1	1.1	2.3	.2	.9	.1	0.0	.2
	76650	.2	1.8	3.1	.1	.2	0.0	.3	0.0	2.3	4.8	.6	2.1	.4	.1	.4
Devonian volcanic & intrusive rocks	GC01-32	.6	34.7	186.9	4.2	11.7	.8	6.7	1.8	30.3	63.0	7.3	31.2	6.5	2.0	6.4
	GC01-38	1.0	47.3	223.1	4.9	16.4	1.1	6.5	1.8	33.3	70.6	8.7	38.9	8.6	2.7	8.9
	GC01-29	2.2	36.8	199.8	5.1	14.0	1.3	14.9	3.8	36.4	77.9	8.2	32.2	6.5	1.2	6.1

Table 1. (Continued)

Tb (ppm)[d]	Dy (ppm)[d]	Ho (ppm)[d]	Er (ppm)[d]	Tm (ppm)[d]	Yb (ppm)[d]	Lu (ppm)[d]	W (ppm)[c]	Sn (ppm)[d]	Bi (ppm)[d]	Mo (ppm)[c]	Au (ppb)[c]	Ag (ppm)[c]	Cu (ppm)[a]	Zn (ppm)[a]	Pb (ppm)[d]	As (ppm)[c]	Sb (ppm)[c]	Hg (ppm)[c]
.2	1.8	.4	1.1	.2	1.0	.2	<4	.9	<0.1	<5	6	<5	58.4	95.8	7.2	<2	5.4	1
.3	1.8	.4	1.1	.2	1.0	.2	<4	.7	<0.1	<5	<5	<5	117.7	68.6	2.3	<2	7.9	<1
1.2	7.8	1.5	4.3	.6	3.8	.6	<4	2.8	<0.1	<5	<5	<5	29.1	117.5	1.8	32	4.8	<1
1.3	8.3	1.6	4.6	.7	4.1	.6	5	3.0	<0.1	<5	<5	<5	25.6	120.9	3.8	15	12.1	<1
.2	1.6	.3	.9	.1	.9	.1	<4	.4	<0.1	<5	<5	<5	52.5	42.3	1.8	71	43.0	<1
.3	1.8	.4	1.0	.1	.9	.1	<4	.4	<0.1	<5	<5	<5	57.5	62.3	1.1	34	26.5	<1
.3	1.8	.4	1.1	.2	1.0	.2	<4	.5	<0.1	<5	6	<5	55.6	59.4	0.7	7	14.9	<1
2.1	15.9	3.7	12.7	1.9	12.8	2.0	30	2.7	<0.1	<5	<5	<5	41.7	353.9	4.2	36	50.4	<1
1.0	6.3	1.3	3.8	.5	3.5	.5	<4	2.5	<0.1	<5	<5	<5	<5.1	98.4	7.8	5	2.9	<1
.6	3.8	.8	2.3	.3	2.0	.3	<4	1.5	<0.1	<5	10	<5	10.1	48.9	8.2	6	2.1	<1
.6	4.1	.8	2.4	.3	2.2	.3	<4	1.8	.2	<5	23	<5	5.8	102.4	25.1	21	12.3	1
.8	5.1	1.0	3.1	.5	3.2	.5	<4	2.4	<0.1	5	<5	<5	7.4	164.4	8.9	17	4.3	<1
.7	4.8	.9	3.0	.4	2.9	.5	<4	1.4	.1	<5	<5	<5	<5.1	80.6	6.2	3	5.9	<1
.7	5.1	1.0	3.2	.5	3.4	.5	<4	1.5	<0.1	<5	<5	<5	<5.1	82.6	2.2	7	4.0	<1
.4	2.9	.5	1.5	.2	1.3	.2	<4	1.2	<0.1	<5	<5	<5	<5.1	71.9	4.1	7	5.2	<1
.4	3.0	.6	1.8	.3	1.9	.3	4	1.6	<0.1	<5	1440	<5	65.4	74.2	3.0	2210	5.8	<1
.2	1.2	.2	.9	.2	1.4	.2	<4	.4	<0.1	<5	133	<5	19.7	13.6	4.2	102	9.5	2
.6	3.9	.8	2.3	.4	2.2	.3	<4	1.3	.2	6	<5	<5	59.3	70.1	7.7	5	0.2	<1
.6	3.8	.8	2.2	.3	2.2	.3	<4	1.5	<0.1	<5	<5	<5	160.4	71.2	6.3	<2	<0.2	<1
.6	3.9	.8	2.4	.4	2.6	.4	<4	1.5	<0.1	<5	5	<5	18.1	42.4	3.5	6	4.7	<1
.5	3.4	.7	1.9	.3	1.8	.3	5	1.2	<0.1	<5	<5	<5	44.1	41.2	10.5	6	11.4	<1
.5	3.5	.7	2.0	.3	1.9	.3	<4	1.6	<0.1	<5	<5	<5	<5.1	44.4	14.2	3	1.5	<1
.5	3.5	.7	2.1	.3	2.1	.3	<4	1.3	<0.1	<5	7	<5	<5.2	47.0	5.5	3	10.8	<1
.5	3.7	.7	2.2	.3	2.2	.3	7	1.4	<0.1	<5	<5	<5	8.0	42.6	3.9	5	12.8	<1
.5	3.2	.7	1.9	.3	1.8	.3	<4	2.5	<0.09	<5	<5	<5	<4.8	107.9	5.6	5	2.7	<1
.6	4.4	.9	2.9	.4	2.9	.5	4	1.5	.6	<5	<5	<5	<5.1	67.5	12.6	8	1.6	<1
.3	1.9	.4	1.3	.2	1.3	.2	7	.6	<0.1	7	1440	<5	20.7	70.4	2.2	3200	5.6	<1
.6	3.8	.8	2.2	.3	2.1	.3	<4	1.6	<0.1	<5	<5	<5	6.7	71.3	10.8	14	12.7	<1
.6	4.0	.8	2.4	.4	2.2	.4	<4	1.4	<0.1	<5	<5	<5	<5.2	82.4	8.0	13	28.7	<1
.8	5.8	1.2	3.7	.5	3.5	.6	5	2.2	.1	<5	<5	<5	<5.2	60.9	8.8	12	16.2	<1
.6	3.8	.8	2.3	.3	2.2	.3	24	1.3	<0.1	<5	1460	<5	65.7	85.3	5.4	8080	40.0	<1
.7	4.7	1.1	3.6	.6	4.3	.7	23	1.4	.1	51	1040	<5	110.8	79.7	5.1	4100	15.9	2
.4	2.8	.6	1.7	.3	1.7	.3	<4	1.2	<0.1	<5	<5	<5	11.1	56.6	5.5	27	9.2	<1
.6	4.0	.8	2.5	.4	2.5	.4	21	1.3	<0.1	6	1170	<5	6.0	54.2	9.5	6030	4.5	<1
.6	3.7	.7	2.2	.3	2.1	.3	14	1.2	<0.1	<5	10	<5	8.0	64.9	3.8	23	22.6	<1
.6	3.6	.7	2.2	.3	2.3	.4	17	1.3	<0.1	14	>5000	<5	<5.1	54.0	4.0	7820	24.4	<1
1.1	7.2	1.4	4.0	.6	3.6	.5	26	1.4	<0.1	<5	>5000	<5	<5.1	105.5	10.6	14 870	40.2	<1
.6	3.8	.8	2.3	.3	2.2	.3	24	1.3	<0.1	<5	1530	<5	9.3	48.8	6.0	5670	21.5	<1
.6	3.6	.8	2.2	.3	2.2	.3	6	1.2	<0.1	<5	53	<5	<5.3	88.3	6.5	79	9.9	<1
.5	3.6	.8	2.3	.4	2.4	.4	7	1.4	<0.1	5	<5	<5	32.4	63.4	2.9	23	5.3	<1
.6	3.9	.8	2.3	.3	2.4	.4	27	1.7	<0.1	<5	>5000	<5	21.0	55.7	2.4	10 520	33.1	<1
.5	3.6	.7	2.1	.3	2.2	.3	15	1.6	<0.1	7	1420	<5	<5.3	47.4	7.7	6240	24.9	1
.5	3.3	.7	2.0	.3	2.0	.3	<4	1.3	<0.1	<5	<5	<5	<5.3	38.7	4.2	26	3.8	<1
.5	3.5	.7	2.1	.3	2.0	.3	19	1.2	<0.1	6	3450	<5	13.4	15.7	3.0	14 020	43.3	<1
0.0	.1	0.0	.1	0.0	.1	0.0	<4	.2	<0.1	<5	23	<5	<5.1	<3.1	-1.3	99	10.3	<1
0.0	.1	0.0	.1	0.0	.1	0.0	<4	.2	<0.1	<5	<5	<5	<5.1	<3.1	-0.8	12	3.5	<1
.1	.6	.1	.4	.1	.4	.1	<4	.4	<0.1	7	400	<5	5.4	439.4	128.7	581	78.9	<1
<0.005	0.0	0.0	0.0	<0.003	0.0	<0.003	<4	.1	<0.1	<5	27	<5	<5.3	10.7	28.1	35	131.0	<1
.3	1.6	.3	.9	.1	.9	.1	5	.9	<0.1	<5	>5000	<5	7.8	433.0	23.7	13 750	48.2	<1
.2	1.4	.3	.8	.1	.7	.1	5	.5	.2	<5	143	<5	46.1	13 163.1	421.0	400	243.0	<1
0.0	.2	0.0	.1	0.0	.1	0.0	<4	.2	.1	6	892	<5	<5.3	51.1	6.4	1990	14.3	<1
0.0	.3	.1	.1	0.0	.1	0.0	<4	.5	.3	5	3900	29	<5.3	<3.2	3.9	10 990	47.7	<1
.9	6.1	1.2	3.4	.5	2.9	.4	<4	1.8	<0.1	<5	7	<5	<5.1	80.2	4.0	<2	0.5	<1
1.2	8.2	1.6	4.5	.6	3.8	.6	<4	2.0	<0.1	<5	17	<5	<5.1	92.7	3.6	3	0.4	<1
.9	6.2	1.2	3.5	.5	3.3	.5	<4	3.6	.3	<5	<5	<5	<5.1	56.3	15.4	<2	1.9	2

Notes

[a]ICP-AES (inductively coupled plasma atomic emission spectrometry); [b]LECO; [c]INAA (instrumental neutron activation analysis); [d]ICP-MS (inductively coupled plasma mass spectrometry); LOI = loss on ignition; ICP-AES and ICP-MS were carried out at Institut National de Recherche Scientifique–Eau, Terre, et Environnement (INRS-ETE), and LECO and INAA were done at XRAL Laboratories.

Abbreviations: Cal = calcite, Ccp = chalcopyrite, cps = counts per second, Hem = hematite, Py = pyrite, Qtz = quartz, Sd = siderite.

described below.

The Porphyritic Felsic Volcanic Unit: This unit consists of massive, porphyritic rocks with locally developed zones of brecciation that contain fragments of porphyritic felsic rocks in a matrix of the same rock type. The massive porphyritic rocks consist of 5% to 30% phenocrysts (typically 0.2–2 mm in long dimension) and 70% to 95% groundmass (≤0.2 mm). The most common phenocrysts are of plagioclase and K-feldspar that are variably altered to sericite ± carbonate; quartz phenocrysts are rare. Patches of leucoxene and associated arsenopyrite and pyrite (replacing phenocrysts of ilmenite?) are common. Pseudomorphs of hornblende and pyroxene replaced by chlorite were observed in some samples. The phenocrysts are generally euhedral to subhedral, and might form glomerocrysts (Fig. 3A), which is indicative of a volcanic or subvolcanic origin rather than volcaniclastic. The groundmass generally exhibits a micropoikilitic texture suggestive of an earlier spherulitic texture or devitrification. Some centimeter-long, millimeter-spaced, pervasive and parallel wavy lines defined by green illite filling microfractures were locally observed, which might reflect a flow texture (Fig. 3B). Most of this unit has been altered to variable degrees. The least-altered rock has a light gray color, whereas the more altered rocks show green (because of chlorite–calcite–quartz alteration) and buff (because of sericite–ankerite–quartz alteration) colors.

The Volcaniclastic Unit: This unit consists of both heterolithic and monolithic volcanic breccias plus ash tuffs and/or flows. The majority of exposures are of monolithic breccias; the rare outcrops of heterolithic breccias consist of variably sized volcaniclastic fragments ranging in composition from intermediate to felsic. The shape of the fragments varies from rounded to angular (Fig. 3C), and their size varies from a few millimeters to tens of centimeters. Adjacent fragments might have jigsaw fit, indicating in situ brecciation. Locally these breccias have a mottled gray and black appearance (Fig. 3C), apparently because of finely disseminated pyrobitumen in the black matrix. The volcaniclastic rocks mainly comprise crystals in an ash matrix. Glass shards and spherulitic textures are well preserved locally. The original glassy matrix has devitrified and has altered to chlorite locally. The devitrified groundmass is generally an order of magnitude finer grained than in the porphyritic felsic volcanic rock. Bedding, indicated by flattening of glassy lapilli and by change of abundance of crystals and color, is observed in a few places. Crystals and crystal fragments generally make up more than 30% of the rock (Fig. 3D). The most abundant crystals and crystal fragments are plagioclase and K-feldspar. Quartz crystals are minor and are commonly embayed. Pseudomorphs of hornblende and pyroxene (completely replaced by chlorite) were observed.

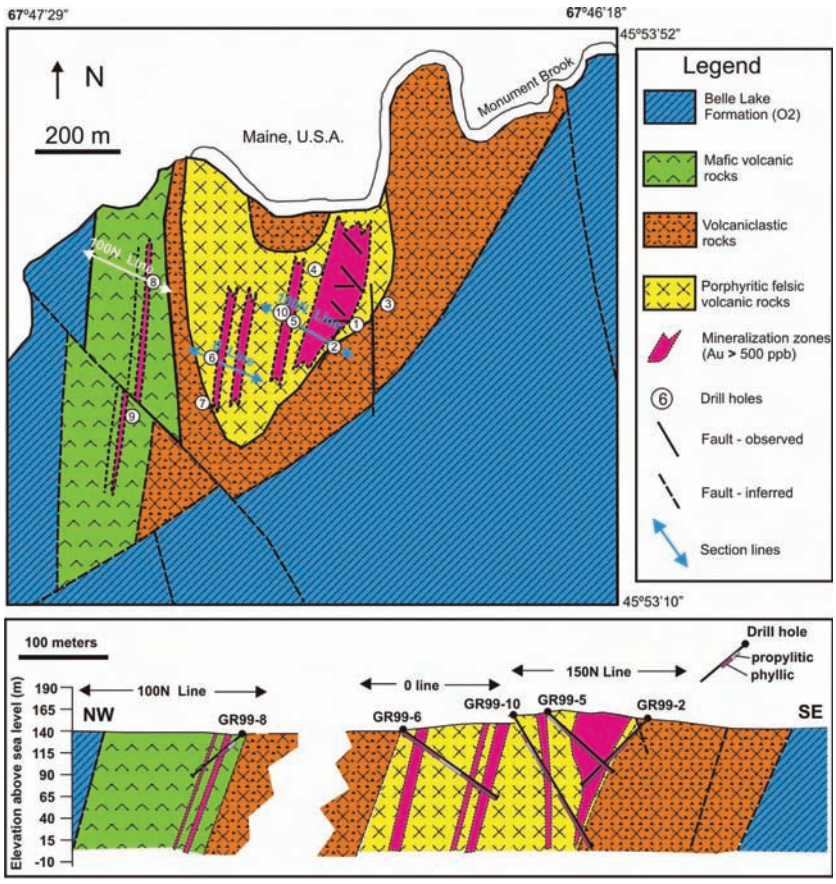

Fig. 2. Local geologic map of Poplar Mountain area, and a composite geologic cross section (modified from Chi and Watters, 2002; Watters and Chi, 2002).

The Mafic Volcanic Unit: This unit consists of dark green-gray, massive, homogeneous basalt and an intercalated subunit composed of centimeter-sized, elongated fragments of volcaniclastic rocks and chert. Two mafic volcanic rock types might be distinguished based on textures. One consists of a fine-grained (0.2–0.3 mm) assemblage of pyroxene, plagioclase, chlorite, titanite, and minor quartz (Fig. 3E), with minor 3 to 4 mm phenocrysts of plagioclase. The other mafic unit is composed of 10% to 15% 1-mm-sized spherules and 85% to 90% very fine grained (0.01–0.02 mm) groundmass (Fig. 3F). Both the spherules and groundmass are composed of pyroxene, indistinct feldspars and quartz (?), titanite, and patches of chlorite. Amygdules filled by calcite and parallel planes containing millimeter-sized, lensoid, blackish spots composed of glass altered to chlorite are common features of this second type.

Relationship Between the Volcanic Units: Fragments of porphyritic felsic

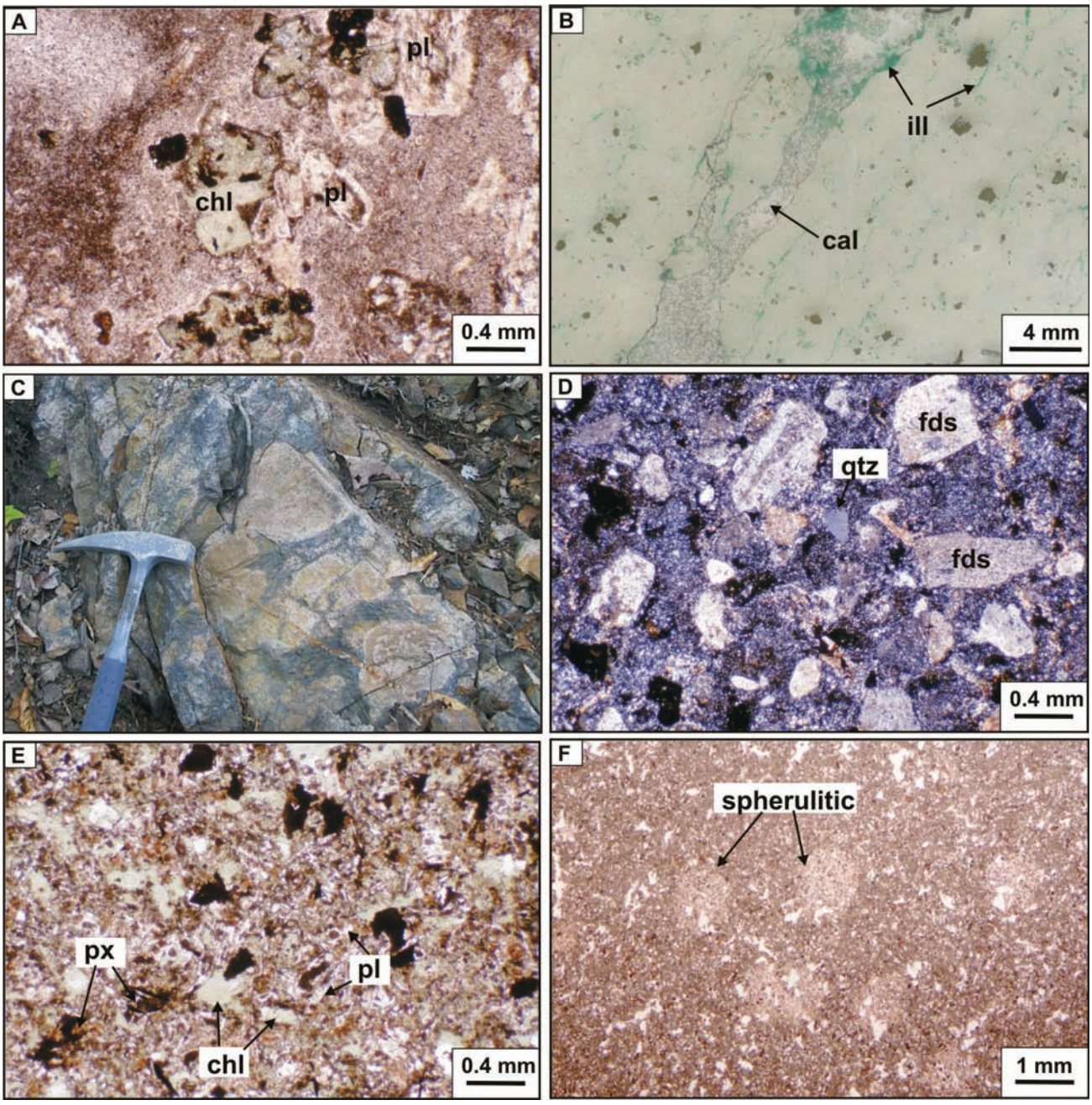

Fig. 3. ***A***. Felsic volcanic unit: photomicrograph of porphyritic texture with glomerocrysts of plagioclase plus hornblende and pyroxene pseudomorphs (replaced by chlorite); sample 01SW34 (plane-polarized light). ***B***. Felsic volcanic unit: parallel wavy lines (filled with green illite) probably reflecting flow textures; sample 01SW31 (scanned thin section). ***C***. Volcaniclastic unit: in situ breccia and mottled texture; outcrop near Trench #1. ***D.*** Volcaniclastic unit: photomicrograph of crystal tuff with abundant crystals and crystal fragments of feldspars and minor quartz; sample GC01-55 (cross-polarized light). ***E***. Mafic volcanic unit: photomicrograph of basalt composed of fine-grained, tabular plagioclase, pyroxene, minor quartz, and glass (altered to chlorite); sample GC01-138 (plane-polarized light). ***F.*** Mafic volcanic unit: photomicrograph of basalt with spherulitic texture; sample GC01-135 (plane-polarized light). Abbreviations: cal = calcite, chl = chlorite, fds = feldspar, ill = illite, pl = plagioclase, px = pyroxene, qtz = quartz.

volcanic rocks have been found locally in the volcaniclastic unit. Therefore the felsic volcanic unit appears to, at least in part, predate the volcaniclastic unit. Two observations indicate that the mafic volcanic unit postdates the other two units: a mafic dike cuts the felsic volcanic unit, and a bed of sedimentary rocks that is intercalated with the mafic volcanic unit contains fragments similar to the volcaniclastic unit (Chi and Watters, 2002).

The porphyritic felsic volcanic unit is located in the center of the volcanic complex, and is surrounded by the volcaniclastic unit, whereas the mafic volcanic unit occurs only on the west side of the complex (Fig. 2). The

porphyritic felsic volcanic unit has been interpreted to be a subvolcanic intrusion based on its overall massive and coherent appearance and porphyritic texture, and has been referred to as "porphyritic dacite" (Watters, 1998; Chi and Watters, 2002; Watters and Chi, 2002). The spatial relationship of the porphyritic felsic volcanic rocks and volcaniclastic rocks is consistent with a volcanic dome, with the porphyritic rocks representing a volcanic plug or a lava dome in an apron of volcaniclastic rocks. Alternatively, the distribution of the lithologic units might reflect a south-plunging anticline (Fig. 2). This latter hypothesis is difficult to verify because the volcaniclastic and mafic volcanic units are poorly exposed, and bedding is rarely observed.

Petrochemical Composition

Major and trace element analyses of volcanic and volcaniclastic rocks from the field area are listed in Table 1. Samples can be divided into least-altered and altered based on petrographic features and chemical composition. The least-altered samples are characterized by relatively low concentrations of carbon, whereas the altered samples show high concentrations of carbon and sulfur (from carbonates and sulfides; see Table 1).

Compositional Classification: The values of major elements shown in Table 1 are normalized to 100% excluding LOI, and are plotted on the total alkali–silica diagram of Le Bas et al. (1986) in Figure 4A. Of the four least-altered mafic volcanic samples, two plot in the field of basalt, and two as basaltic andesite. Compositions of the volcaniclastic rocks are highly variable, scattering from trachybasalt, basaltic andesite, trachyandesite, trachydacite, dacite, to rhyolite. The least-altered felsic volcanic rocks mainly fall in the field of rhyolite, and near the rhyolite/dacite boundary. In contrast, most of the altered felsic volcanic rocks fall in the field of dacite.

Because silica and alkali are sensitive to alteration, even the least-altered samples can only provide an approximation of the rock types using the above classification scheme. An alternative method for rock classification in altered rocks is the immobile element diagram of Winchester and Floyd (1977; Fig. 4B). On this diagram, altered and least-altered felsic volcanic rocks are indistinguishable, both clustering in the rhyodacite–dacite field, near the boundary with andesite. The volcaniclastic rocks straddle the boundary between the rhyodacite–dacite and andesite fields, whereas the mafic rocks plot in the alkali and subalkaline basalt fields.

Petrochemical Comparison with Other Volcanic Rocks in the Region: Petrochemical data of the PMVC rocks are compared to those of other volcanic rocks in the region, i.e., the Devonian volcanic rocks of the Tobique Group in the Canterbury basin and the Ordovician volcanic rocks of the Meductic Group in the Miramichi terrane, to distinguish them geochemically. Petrochemical data of the Ordovician volcanic rocks, including felsic (Porten Road Formation), intermediate (Eel River Formation), and mafic (Oak Mountain Formation), are from Fyffe (2001). The data for the Devonian volcanic rocks from the Canterbury basin were obtained in this study, including two samples of mafic volcanic rocks of the Dorrington Hill Formation, and one sample of felsic rock of the Dow Porphyry (Table 1).

In Figure 5, chondrite-normalized rare earth element

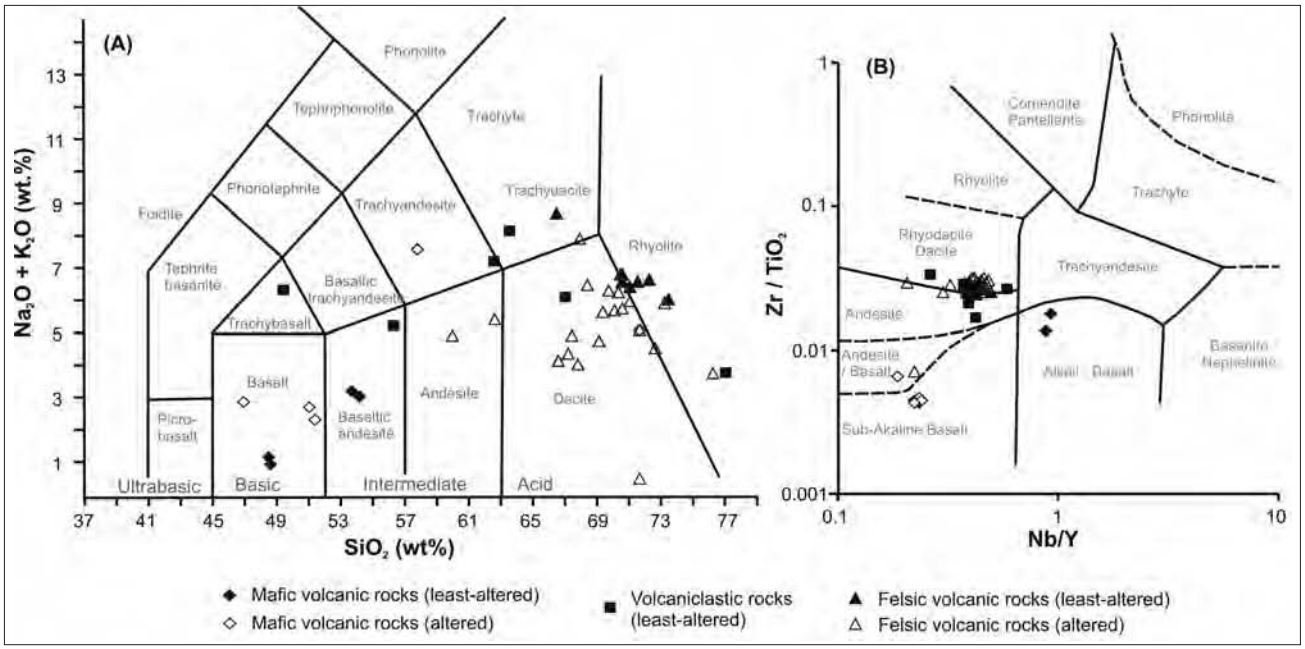

Fig. 4. Compositional classification of the volcanic and volcaniclastic rocks from Poplar Mountain. ***A***. Total alkali–silica classification scheme of Le Bas et al. (1986). ***B***. Zr/TiO_2 vs. Nb/Y diagram of Winchester and Floyd (1977), showing both least-altered (filled symbols) and altered (open symbols) samples.

(REE) patterns for volcanic and volcaniclastic rocks of Poplar Mountain overlap partly with the Ordovician Meductic Group, and partly with the Devonian Dorrington Hill Formation and Dow porphyry. They are all characterized by light rare earth element (LREE) enrichment and by minor Eu depletion for the felsic components. The REE patterns of the Poplar Mountain samples lie between those of the Ordovician and Devonian samples.

Using trace element granitic composition discrimination diagrams of Pearce et al. (1984), the porphyritic felsic volcanic rocks and volcaniclastic rocks of Poplar Mountain fall in the same fields (volcanic arc granite) as the Meductic Group and Dow porphyry (Fig. 6). On the Nb–Y diagram, they all fall in the syn-collisional and volcanic arc granites field (Fig. 6A), and on the Ta–Yb diagram, they fall in the field of volcanic arc granites (Fig. 6B). The Dow porphyry is close to the within-plate granites boundary, the Meductic samples spread away from the boundary, and the Poplar Mountain samples overlap the Meductic samples and cluster toward the boundary (Fig. 6).

Geochronology

One sample (GC01-40; GSC Lab number = Z7083) of the porphyritic felsic volcanic rock from Poplar Mountain was collected for U–Pb isotopic dating. Very few zircons were recovered and these exhibited a range of morphologies consistent with an inherited origin. The zircons were analyzed on the GSC SHRIMP II ion probe. Among the analyzed 18 zircons, 16 have late Ordovician ages that cluster around a mean value of 459 Ma (Fig. 7). Although these analyses define one statistical population, the diversity of grain types found in the sample, and range of compositions suggest that these grains are most likely inherited. Two grains (#43 and #53), which contained inclusions of alkali feldspar and quartz and appeared different from the dominant zircon types in the rock, yielded significantly younger ages of ca. 390 Ma (Table 2).

Mineralization and Alteration

The Poplar Mountain gold occurrence contains several zones of gold mineralization (Fig. 2). Channel samples have yielded up to 1.2 g/t Au over 28 m at surface, whereas drill intersections yield up to 2.5 g/t Au over 13.4 m (Freewest Resources Canada Inc., unpub. report, 1999). Gold mineralization known so far is mainly hosted in the porphyritic felsic volcanic rock, and to a lesser extent in the mafic volcanic rocks, which have returned values of up to 1.1 g/t Au over 6.6 m. The mineralization in the mafic rocks is located mainly along the contact zones with intercalated volcano-sedimentary rocks. The distribution of the mineralized zones (Fig. 2) is based on assay data and inferences from ground magnetic data (Freewest Resources Canada Inc., unpub. report, 1999). In vertical extent, it appears that the easternmost mineralized zone narrows with depth (Fig. 2).

Mineralization Styles

The gold-mineralization zones outlined by assay data

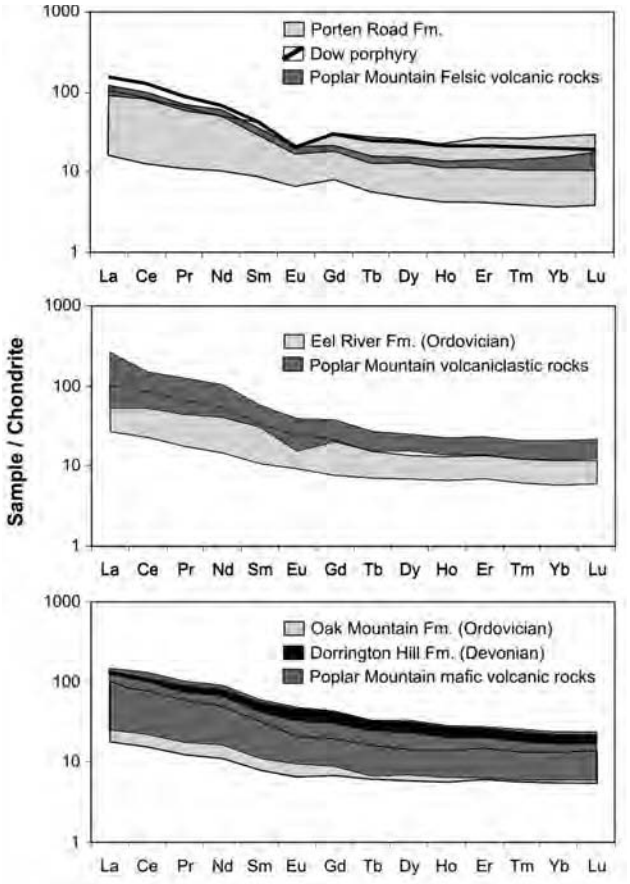

Fig. 5. REE patterns for volcanic and volcaniclastic rocks from Poplar Mountain, compared with Ordovician Meductic Group volcanic rocks, Devonian Dorrington Hill Formation volcanic rocks, and Dow porphyry. Chondrite normalization factors are from Evensen et al. (1978).

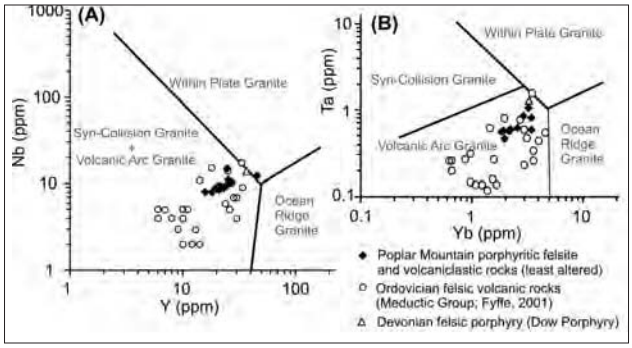

Fig. 6. Trace element diagrams discriminating different tectonic environments (Pearce et al., 1984). Data for felsic volcanic and volcaniclastic rocks from Poplar Mountain are compared with the Ordovician Meductic Group felsic volcanic rocks and Devonian Dow porphyry.

are invariably characterized by enrichment of arsenopyrite. Gold is inferred to be contained in arsenopyrite as ionic substitution or submicron-sized grains because no visible gold was found in hand samples or thin sections. Arsenopyrite is disseminated in the host rocks (Fig. 8A,B), in quartz-carbonate-sericite veins or stockworks (Fig. 8A,C), and in both the fragments and matrix of breccias (Fig.

Table 2. SHRIMP U/Pb Zircon Results for Sample GC01-144

Spot Name	U (ppm)	Th (ppm)	Th/ U	Pb* (ppm)	^{204}Pb (ppm)	^{204}Pb/ ^{206}Pb	±^{204}Pb/ ^{206}Pb	$f(206)^{204}$	^{208*}Pb/ ^{206*}Pb	±^{208}Pb/ ^{206}Pb	^{207*}Pb/ ^{235}U	±^{207}Pb/ ^{235}U	^{206*}Pb/ ^{238}U	±^{206}Pb/ ^{238}U	Corr Coeff	^{207*}Pb/ ^{206*}Pb	±^{207}Pb/ ^{206}Pb	Apparent Ages (Ma) ^{206}Pb/ ^{238}U	±^{206}Pb/ ^{238}U	^{207}Pb/ ^{206}Pb	±^{207}Pb/ ^{206}Pb	Disc. (%)
GC01-144 Zircon (NAD83; Zone 19 594482; 5082801)																						
7083-2.1	306	168	0.57	24	8	0.000426	0.000128	0.00738	0.1697	0.0082	0.5338	0.0311	0.07405	0.00140	0.4380	0.05229	0.00276	461	8	298	125	155
7083-3.1	102	50	0.50	8	2	0.000247	0.000274	0.00428	0.1556	0.0139	0.5681	0.0501	0.07431	0.00124	0.3084	0.05545	0.00469	462	7	430	200	107
7083-4.1	205	131	0.66	17	0	0.000010	0.000010	0.00017	0.2164	0.0084	0.5688	0.0138	0.07364	0.00106	0.6867	0.05602	0.00099	458	6	453	40	101
7083-6.1	176	135	0.79	14	0	0.000004	0.000094	0.00007	0.2462	0.0093	0.5726	0.0199	0.07191	0.00094	0.4865	0.05775	0.00177	448	6	520	69	86
7083-11.1	115	54	0.49	9	1	0.000121	0.000140	0.00210	0.1616	0.0103	0.5363	0.0276	0.07258	0.00109	0.4066	0.05358	0.00254	452	7	354	111	128
7083-12.1	186	96	0.53	15	4	0.000302	0.000166	0.00523	0.1708	0.0115	0.5642	0.0348	0.07438	0.00100	0.3368	0.05502	0.00322	463	6	413	137	112
7083-16.1	424	524	1.27	39	2	0.000069	0.000065	0.00120	0.3673	0.0132	0.5700	0.0184	0.07424	0.00107	0.5528	0.05569	0.00151	462	6	440	61	105
7083-18.1	246	98	0.41	18	0	0.000010	0.000010	0.00017	0.1322	0.0059	0.5795	0.0183	0.07356	0.00098	0.5306	0.05713	0.00154	458	6	497	60	92
7083-19.1	176	96	0.56	14	3	0.000305	0.000138	0.00528	0.1647	0.0090	0.5318	0.0269	0.07332	0.00110	0.4110	0.05260	0.00244	456	7	312	109	146
7083-23.1	285	223	0.81	24	0	0.000001	0.000074	0.00002	0.2634	0.0081	0.5967	0.0181	0.07540	0.00097	0.5320	0.05739	0.00149	469	6	507	58	93
7083-24.1	239	265	1.15	21	2	0.000106	0.000108	0.00185	0.3526	0.0119	0.5551	0.0213	0.07243	0.00092	0.4437	0.05559	0.00192	451	6	436	79	103
7083-26.1	293	220	0.77	24	1	0.000057	0.000036	0.00098	0.2380	0.0071	0.5811	0.0130	0.07401	0.00087	0.6254	0.05694	0.00100	460	5	489	39	94
7083-38.1	326	149	0.47	25	2	0.000120	0.000066	0.00208	0.1385	0.0146	0.5566	0.0155	0.07390	0.00088	0.5334	0.05463	0.00130	460	5	397	54	116
7083-48.1	914	1658	1.87	97	1	0.000025	0.000028	0.00043	0.5935	0.0064	0.5797	0.0095	0.07423	0.00080	0.7438	0.05664	0.00063	462	5	477	25	97
7083-50.1	72	45	0.65	6	2	0.000340	0.000246	0.00589	0.2015	0.0161	0.5490	0.0447	0.07268	0.00155	0.3780	0.05478	0.00416	452	9	403	180	112
7083-54.1	503	358	0.74	41	3	0.000090	0.000068	0.00157	0.2266	0.0056	0.6129	0.0152	0.07430	0.00086	0.5720	0.05983	0.00122	462	5	597	45	77
7083-43.1	546	296	0.56	36	0	0.000010	0.000010	0.00017	0.1702	0.0049	0.4737	0.0105	0.06309	0.00091	0.7342	0.05446	0.00083	394	6	390	34	101
7083-43.2	987	1370	1.43	79	2	0.000038	0.000030	0.00066	0.4529	0.0065	0.4590	0.0094	0.06121	0.00087	0.7714	0.05439	0.00071	383	5	387	30	99
7083-43.3	484	254	0.54	32	2	0.000088	0.000049	0.00152	0.1783	0.0056	0.4699	0.0107	0.06216	0.00072	0.6100	0.05483	0.00100	389	4	405	41	96
7083-53.1	440	588	1.38	35	1	0.000027	0.000099	0.00047	0.4121	0.0096	0.4680	0.0206	0.06221	0.00076	0.3928	0.05455	0.00222	389	5	394	94	99

Notes

Uncertainties reported at 1s (absolute) and are calculated by numerical propagation of all known sources of error.

$f(206)^{204}$ refers to mole fraction of total ^{206}Pb that is due to common Pb, calculated using the ^{204}Pb-method; common Pb composition used is the surface blank.

Discordance relative to origin = 100 * (1–(^{206}Pb/^{238}U age)/(^{207}Pb/^{206}Pb age)).

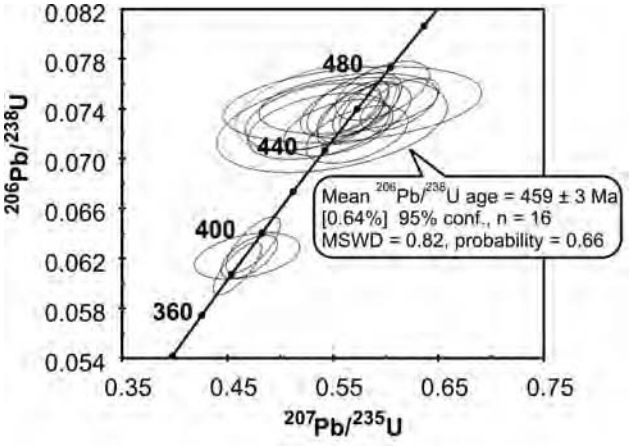

Fig. 7. $^{206}Pb/^{238}U$ vs. $^{207}Pb/^{235}U$ diagram showing the range of ages obtained from zircons from the felsic volcanic unit of Poplar Mountain (GC01-40).

8D). Minor amounts of sphalerite and stibnite occur in some quartz-carbonate veins. Globules of pyrobitumen are locally conspicuous in the quartz-carbonate-sericite veins in some gold-mineralized zones. Arsenopyrite is typically acicular and disseminated (Fig. 8B,C), being volumetrically minor in veins. The mineralized zones are generally characterized by brittle structures, but in the lower parts of some drill cores (GR99-10), arsenopyrite appears to be distributed along foliations outlined by carbonate and sericite (Fig. 8E,F). The quartz-carbonate-sericite veins are generally millimeters to centimeters wide, and a few are tens of centimeters wide. There is no clear geologic or structural boundary between mineralized and non-mineralized zones, although the mineralized zones are characterized by a higher concentration of quartz-carbonate-sericite veining than the barren zones.

Element Associations

The samples analyzed contain <5 ppb to >5000 ppb Au (Table 1). Au correlates positively with As with a Pearson correlation coefficient of 0.96 (Fig. 9A), as has been noted previously (e.g., Watters, 1998). A weak positive correlation seems to exist between Au and S ($r = 0.55$; Fig. 9B), and Au and Sb ($r = 0.53$; Fig. 9D). Au is not correlative to other elements, including C, Sn, and Zn (Fig. 9C,E,F), and W, Bi, Mo, Cu, and Pb (Table 1). Ag and Hg are generally lower than 5 ppm and 2 ppm, respectively, regardless of Au contents.

Alteration Types and Paragenesis

Two types of alteration can be distinguished based on mineral assemblages and crosscutting relationships. The first type consists of chlorite, calcite, and quartz, with minor illite and pyrite, whereas the second type consists of sericite, ankerite, and quartz, with minor illite and pyrite. Petrographic evidence (Fig. 10; e.g., sericite replacing calcite and chlorite, and ankerite veinlets cutting calcite) invariably indicates that the chlorite–calcite–quartz alteration predates the sericite–ankerite–quartz alteration. Arsenopyrite is always associated with sericite, ankerite, and quartz (Fig. 8C,F), and never with calcite and chlorite. The chlorite–calcite–quartz alteration is best preserved in non-mineralized areas, whereas it is largely replaced by sericite–ankerite–quartz alteration in mineralized zones (Fig. 2), further supporting that the sericite–ankerite–quartz alteration is related to gold mineralization, whereas the chlorite–calcite–quartz alteration predates mineralization.

Age of Mineralization

The spatial relationship between arsenopyrite and sericite–ankerite–quartz alteration as discussed above implies that they are coeval. Therefore, the age of mineralization can be determined if the radiometric age of sericite can be ascertained. Sericite occurs as disseminations in the host rocks or as very thin coatings on vein walls (Fig. 8C). However, massive sericite occurs in a vein where it replaces calcite in sample GC01-74 (from drill hole GR99-10, at a downhole depth of 26.5 m; Fig. 10D,E). The sericite separated from this sample for $^{40}Ar/^{39}Ar$ analysis forms composite grains consisting of finer individual crystals. Argon isotopic data are listed in Table 3, and presented as a spectrum of gas release (Fig. 11). The data define a plateau age of 411 ± 3.7 Ma, with minor disturbance observed only in the lower temperature increments.

Geochemistry of Alteration

Alteration has brought about significant chemical changes to the host rocks. These changes are difficult to evaluate quantitatively because of the lack of unaltered samples and the lithological variability of the host rocks. Nevertheless, a comparison of the least-altered and altered felsic volcanic rocks reveals certain systematic changes (Fig. 12). Specifically, SiO_2 is lower in altered than least-altered rocks (Figs. 4, 12), whereas Al_2O_3 does not show a systematic change (Fig. 12). Altered rocks are generally higher in S, C, W, Sb, As, and Au than least-altered rocks (Fig. 12).

A set of three samples of altered basalt, showing different degrees of sericite–ankerite–quartz alteration over a short distance (15 cm), are particularly useful for evaluating the chemical changes during the sericite–ankerite–quartz alteration. From least to most altered, these samples are GC01-127-3, GC01-127-2, and GC01-127-1 (see Table 1 for details). With increasing degree of sericite–ankerite alteration accompanied by decreasing chlorite, the color changes from light to medium green, through light green to buff, to buff. Potential immobile components TiO_2, Zr, and Al_2O_3 form a well-defined isocon (Fig. 13A; method of Grant, 1986), and Al_2O_3 was used as an immobile component in mass balance calculation using the equations of Gresens (1967). The net changes of components or elements that show systematic changes from least-altered to most altered are presented in Figure 13B, where the net changes refer to the change relative to the least-altered sample in percentage (see Lentz and Gregoire, 1995). Fe_2O_3, MnO and MgO are close to the isocon and show slight depletion (lost from the system), Na_2O and to a lesser extent SiO_2 are more depleted, and CaO, K_2O, S, C, Ba, Sr, Rb, Cs, Pb, As, and Sb are significantly enriched (added to the system; Fig. 13).

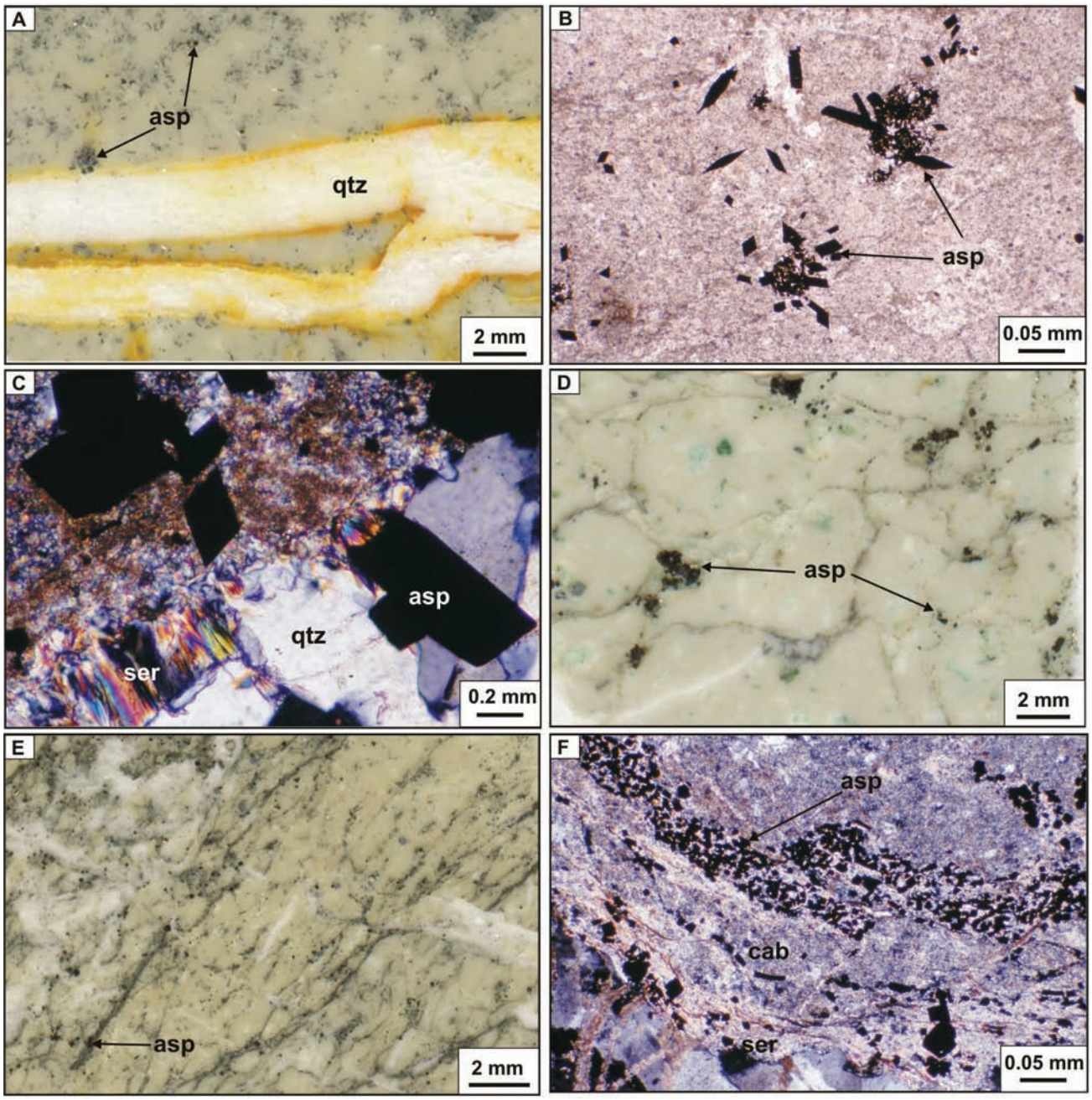

Fig. 8. Photomicrographs showing various mineralization styles. ***A***. Arsenopyrite disseminated in felsic volcanic rock and on the wall of a quartz vein (sample 97SW46; scanned thin section). ***B***. Acicular arsenopyrite disseminated in felsic volcanic rock (sample 97SW46; plane-polarized light). ***C***. An arsenopyrite crystal growing on the wall of a quartz-sericite vein (sample 97SW46; cross-polarized light). ***D***. Brecciated felsic volcanic rock with arsenopyrite distributed in the matrix and the fragments (sample GC01-69; scanned thin section). ***E***. Arsenopyrite distributed along foliation in felsic volcanic rock (sample GC-01-62; scanned thin section). ***F***. Association of arsenopyrite with carbonate and sericite (sample GC-01-62; cross-polarized light). Abbreviations: asp = arsenopyrite; cab = carbonate; qtz = quartz; ser = sericite.

Structure

Overall, the host rocks of the gold mineralization are characterized by brittle deformation, including fracturing and brecciation. Foliation defined by preferential orientation of sericite is observed in the deeper part of a few drill cores, and closely spaced (centimeter-scale) parallel fractures with thin quartz ± carbonate ± sericite vein fillings are widespread. Their orientations are fairly consistent at outcrop scale, but highly variable at prospect scale (Chi and Watters, 2002). As mentioned above, there are no clear geologic or structural boundaries between ore and non-ore zones. The orientation of the mineralized zones presented in Fig. 2 is mainly based on a ground magnetic map (Freewest Resources Canada Inc., unpub. report, 1999). Several NW- and E–W-trending faults, with associated gold

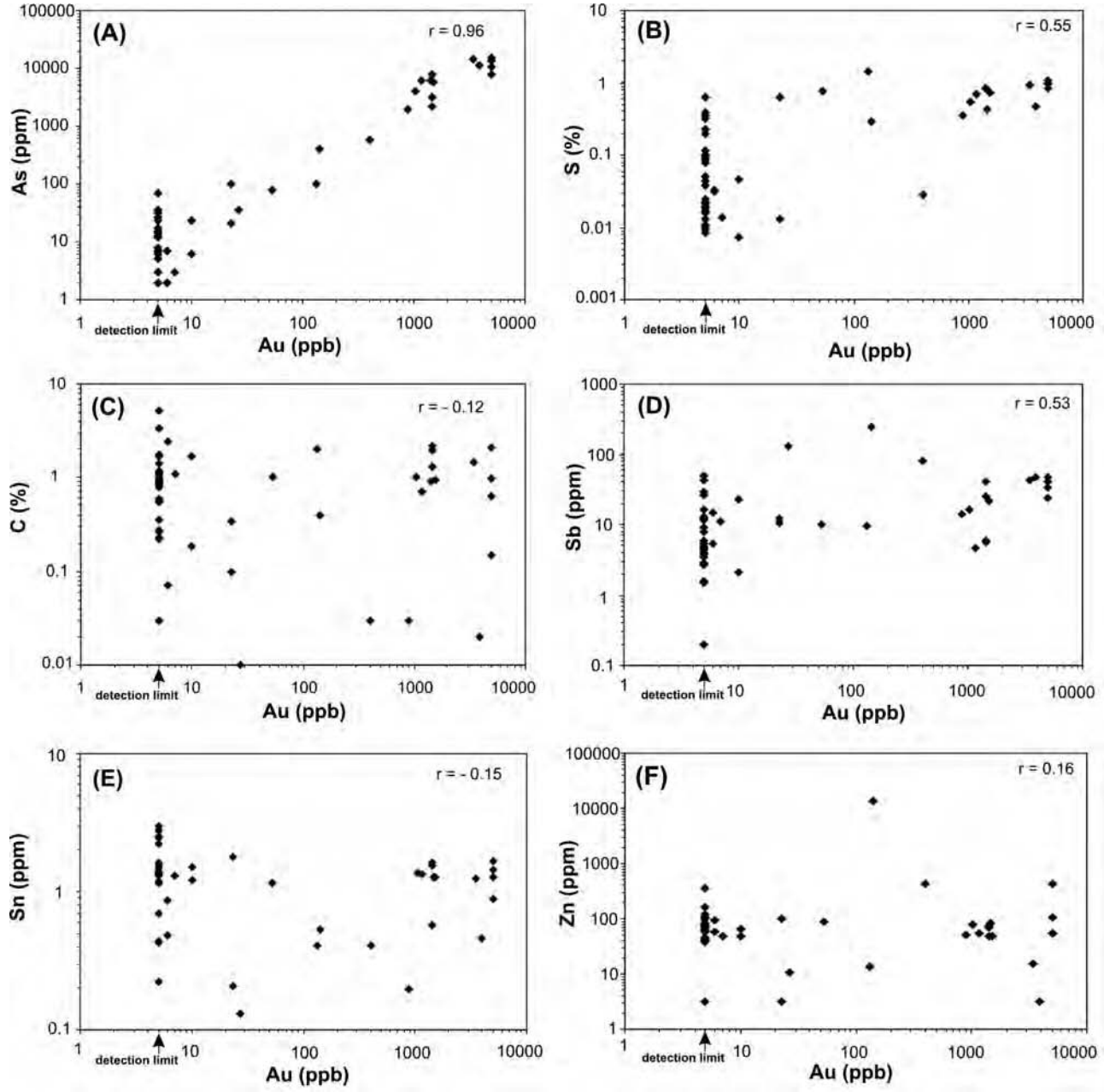

Fig. 9. Abundance relationships between Au and As (***A***), S (***B***), C (***C***), Sb (***D***), Sn (***E***), and Zn (***F***); *r* = Pearson correlation coefficient.

mineralization in veins and breccias, occur in the largest mineralized zone (Fig. 2). Subsidiary fractures associated with these faults and slickensides/fibers on the fault planes commonly indicate sinistral strike-slip movements along the NW- and NNW-trending faults and dextral strike-slip movements along the E–W-striking faults (Watters, 1998). The orientation of these faults and the movement senses indicate that they are conjugate and related to NW–SE oriented shortening (Chi and Watters, 2002).

Fluid Inclusions

Fluid Inclusion Types, Petrography, and Microthermometry

Fluid inclusions from pre-Au mineralization calcite and quartz and syn-Au mineralization quartz and ankerite can be divided into three types: type 1 aqueous inclusions homogenizing into the liquid phase with no carbonic components detectable by microthermometry; type 2 aqueous-carbonic inclusions homogenizing into the aqueous liquid phase; and type 3 carbonic-aqueous inclusions homogenizing into the carbonic vapor phase. Type 2 inclusions can be further divided into subtype 2a inclusions having a carbonic concentration high enough to allow the melting and homogenization temperatures of the carbonic phases to be measured, and subtype 2b inclusions whose carbonic con-

Table 3. $^{40}Ar/^{39}Ar$ Analytical Results for Sericite (Sample GC01-74)

Power[a]	Volume $^{39}Ar \times 10^{-11}$ cc	$^{36}Ar/^{39}Ar$	$^{37}Ar/^{39}Ar$	$^{38}Ar/^{39}Ar$	$^{40}Ar/^{39}Ar$	% ^{40}Ar ATM	$^{40}Ar^{b}/^{39}Ar$	f_{39}[c] (%)	Apparent Age (Ma)[d]
GC01-74 Sericite; J=.02358070 (NAD83; Zone 19 594484; 5082794)[e]									
2.4	5.321	0.0018 ± 0.0005	0.055 ± 0.002	0.009 ± 0.011	10.009 ± 0.058	5.2	9.487 ± 0.110	1.2	364.23 ± 3.84
2.6	14.979	0.0005 ± 0.0002	0.093 ± 0.004	0.003 ± 0.011	10.784 ± 0.045	1.2	10.657 ± 0.054	3.3	404.45 ± 1.83
2.8	7.953	0.0005 ± 0.0003	0.529 ± 0.048	0.003 ± 0.011	10.849 ± 0.063	1.1	10.725 ± 0.091	1.8	406.75 ± 3.10
3.0	37.546	0.0001 ± 0.0001	0.205 ± 0.009	0.002 ± 0.011	10.804 ± 0.021	0.4	10.764 ± 0.028	8.3	408.07 ± 0.94
3.3	33.478	0.0001 ± 0.0001	0.009 ± 0.001	0.002 ± 0.011	10.855 ± 0.022	0.3	10.823 ± 0.027	7.4	410.06 ± 0.91
3.5	98.921	0.0001 ± 0.0000	0.004 ± 0.000	0.002 ± 0.011	10.856 ± 0.019	0.2	10.830 ± 0.020	21.8	410.32 ± 0.67
3.9	107.588	0.0001 ± 0.0000	0.003 ± 0.000	0.002 ± 0.011	10.893 ± 0.030	0.2	10.866 ± 0.030	23.7	411.53 ± 1.02
4.2	40.494	0.0001 ± 0.0001	0.006 ± 0.001	0.002 ± 0.011	10.885 ± 0.040	0.2	10.859 ± 0.043	8.9	411.31 ± 1.47
4.6	31.032	0.0001 ± 0.0001	0.006 ± 0.000	0.002 ± 0.011	10.867 ± 0.020	0.2	10.851 ± 0.025	6.8	411.03 ± 0.86
5.0	24.173	0.0001 ± 0.0001	0.008 ± 0.001	0.001 ± 0.011	10.891 ± 0.032	0.2	10.874 ± 0.041	5.3	411.80 ± 1.39
6.0	39.304	0.0000 ± 0.0001	0.006 ± 0.000	0.002 ± 0.011	10.868 ± 0.030	0.1	10.858 ± 0.032	8.7	411.26 ± 1.10
12.0	13.128	0.0001 ± 0.0002	0.014 ± 0.001	0.002 ± 0.011	10.898 ± 0.048	0.2	10.875 ± 0.067	2.9	411.82 ± 2.27

Notes
[a]As measured by laser in % of full nominal power (10W).
[b]Radiogenic ^{40}Ar, as measured by laser in % of full nominal power (10W).
[c]Fraction ^{39}Ar as percent of total run.
[d]Errors are analytical only and do not reflect error in irradiation parameter J.
[e]Nominal J, referenced to FCT-SAN = 28.03 Ma (Renne et al., 1994).
All uncertainties quoted at 2σ level.

centration is so low that its presence is only demonstrated by the melting of clathrates. For the type 3 inclusions, the aqueous phase is not visible in many cases. A schematic representation of the fluid inclusion types, along with some examples, are presented in Figure 14.

In all the samples examined, no definite relationship between fluid inclusion entrapment and crystal growth can be established, and so no fluid inclusions can be assigned to the primary category with certainty. It is possible that fluid inclusions occurring in clusters (Fig. 14B,D), in isolation (Fig. 14C), along short trails within crystals (Fig. 14E), or in random distribution might represent primary or pseudosecondary fluid inclusions, but a secondary origin for some of them cannot be ruled out. Only type 1 fluid inclusions occur in pre-mineralization calcite and quartz, whereas types 1, 2a, 2b, and 3 occur in the mineralization-stage quartz and ankerite.

In most cases, the liquid:vapor ratios of fluid inclusions within individual fluid inclusion assemblages (clusters, short trails) are consistent (Fig. 14B,D,E), suggesting homogeneous trapping. In some cases, however, the liquid: vapor ratios of fluid inclusions within a given fluid inclusion assemblage are highly variable (Fig. 14F), suggesting necking or heterogeneous trapping. In such cases, microthermometric measurements were not made.

The microthermometric results are listed in Table 4 for individual fluid inclusion assemblages or isolated fluid inclusions. The results are discussed separately below in terms of premineralization- and mineralization-stage minerals.

Fluid Inclusions in Premineralization Calcite and Quartz

As discussed above, only type 1 fluid inclusions (aqueous fluid inclusions homogenizing into the liquid phase) occur in the premineralization calcite and quartz. The final melting temperatures of ice range from –0.1° to –4.5°C (Table 4 and Fig. 15A), corresponding to salinities of 0.2 to 7.2 wt.% NaCl equivalent based on the equation of Bodnar (1993). The homogenization temperatures range from 116° to 159°C (Fig. 15B).

Fluid Inclusions in Mineralization-Stage Quartz and Ankerite

All three types of fluid inclusions described above occur in the Au-related quartz and ankerite, although type 2 fluid inclusions are dominant.

The melting temperatures of CO_2 (Tm_{CO_2}) were measured for type 3 and type 2a fluid inclusions. They range from –56.8° to –57.5°C and from –56.6° to –57.3°C, respectively (Table 4; Fig. 16A). These melting temperatures suggest that the carbonic phase contains variable amounts of other gases in addition to CO_2. Tm_{CO_2} values of type 3 fluid inclusions largely overlap with type 2 fluid inclusions (Fig. 16A), suggesting that they have similar composition.

The melting temperatures of ice (Tm_{H_2O}) of type 1 fluid inclusions range from –1.8° to –5.2°C, corresponding to salinities of 3.1 to 8.1 wt.% NaCl equivalent as calculated with the equation of Bodnar (1993; Table 4). The melting temperatures of clathrates were measured for type 2a and type 2b fluid inclusions. They range from +4.6° to +10.8°C and from +5.6° to +10.8°C, respectively, but mainly from +7.6° to +8.8°C (Fig. 16B). These clathrate melting temperatures for type 2a inclusions correspond to salinities of 2.3 to 10.6 wt.% NaCl equivalent, with most falling between 2.3 and 5.6 wt.% NaCl equivalent (calculated using the program "Clathrates" by Bakker, 1997). The salinities of type 2b inclusions were not calculated because neither Tm_{H2O} nor $Tm_{clathrate}$ can be used: Tm_{H2O} would yield salinity values higher than the real salinities because some water was taken by the clathrate, and $Tm_{clathrate}$ must be

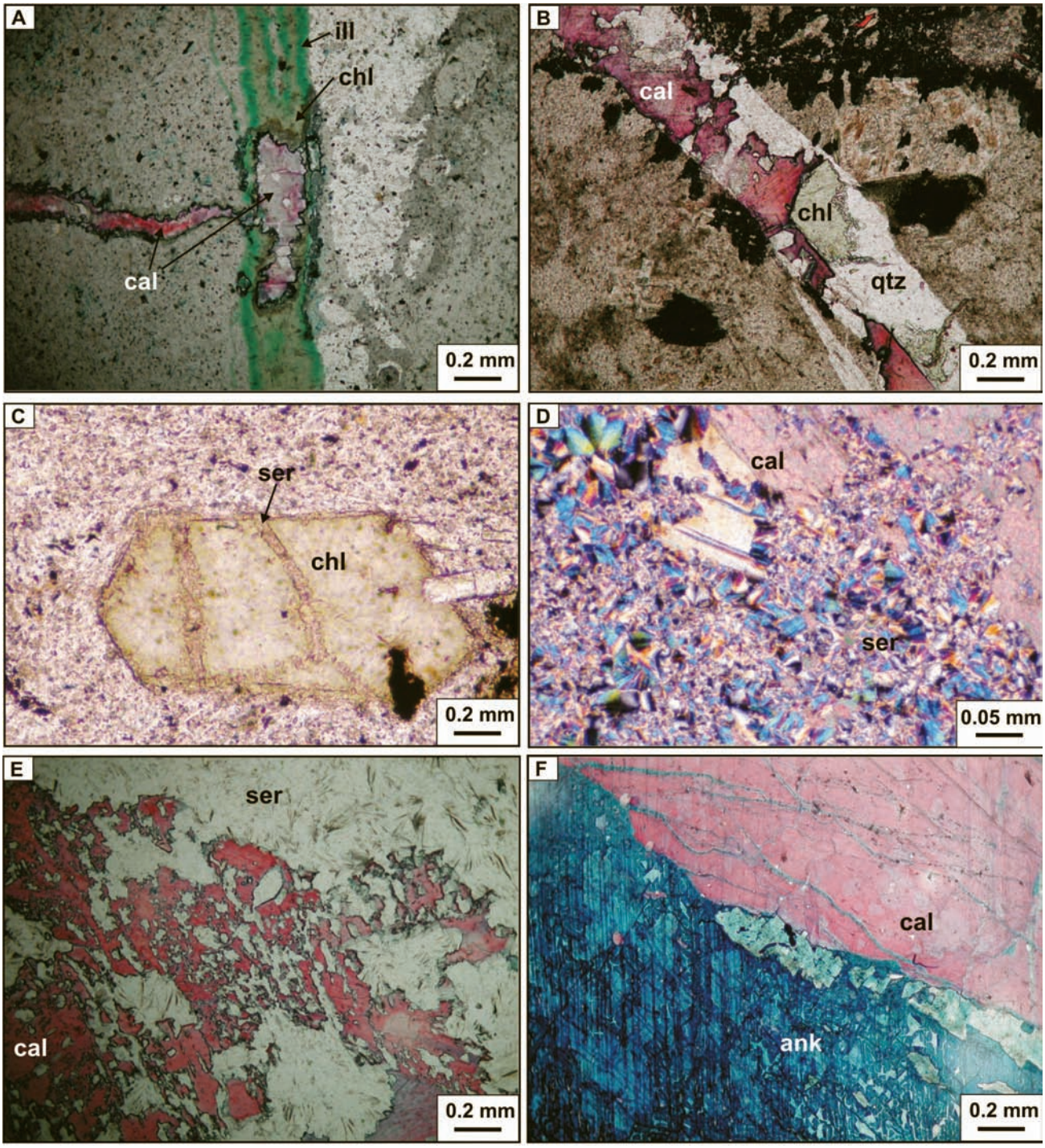

Fig. 10. Photomicrographs showing two alteration types and their crosscutting relationships. ***A***. Illite–chlorite–calcite (stained red) vein (sample GC01-70; plane-polarized light). ***B***. Chlorite–calcite (stained red)–quartz vein (sample 01SW46; plane-polarized light). ***C***. Chlorite replacing a phenocryst in felsic volcanic rock, and cut by sericite (sample GC01-79; plane-polarized light). ***D***. Sericite replacing calcite (sample GC01-74; cross-polarized light). E. Sericite replacing red-stained calcite (sample GC01-74; plane-polarized light). F. Ankerite (stained blue) cutting calcite (stained red; sample 01SW38; plane-polarized light). Abbreviations: ank = ankerite; cal = calcite; chl = chlorite; ill = illite; qtz = quartz; ser = sericite.

coupled with $ThCO_2$ (unavailable for type 2b inclusions) to calculate salinities.

The homogenization temperatures of the carbonic phases were measured for type 2a and type 3 fluid inclusions, and with the exception of a few type 2a fluid inclusions, which homogenized into the carbonic vapor phase (Fig. 16C), most homogenized into the carbonic liquid phase: 25.1° to 30.2°C for type 2a, and 15.9° to 28.1°C for type 3 inclu-

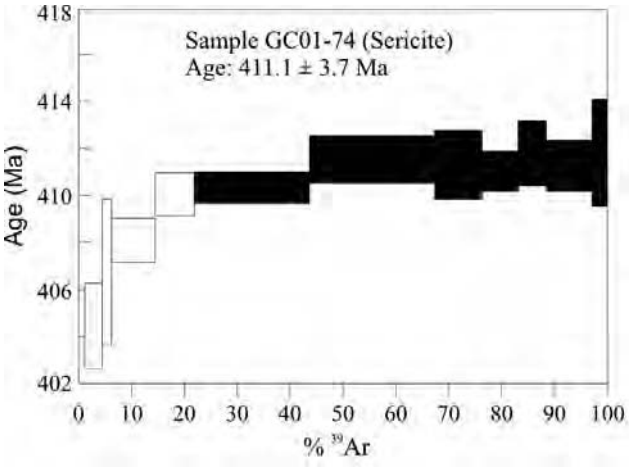

Fig. 11. $^{39}Ar/^{40}Ar$ incremental heating spectrum of sericite (Sample GC01-74). The black steps are those used in the plateau age calculation.

sions (Fig. 16C).

The temperatures of final homogenization of types 1, 2a, and 2b fluid inclusions, all of which homogenize into the liquid phase, range from 113° to 273°C, 221° to 268°C, and 175° to 279°C, respectively. A major overlap among the three types occurs between 220° and 270°C (Fig. 16D). The homogenization temperatures of type 3 fluid inclusions cannot be measured because the aqueous phase is invisible in most cases.

Raman Microspectroscopic Results

The volatile composition of the vapor phase of fluid inclusions has been analyzed by laser Raman spectroscopy. Fluid inclusions from premineralization quartz (type 1) and a few from mineralization-stage quartz contain no volatiles other than H_2O. Most fluid inclusions from the mineralization-stage quartz, both types 2 and 3, show a volatile composition dominated by CO_2, accompanied by significant amounts of N_2 and trace amounts of CH_4 (Table 5 and Fig. 17). These results confirm the microthermometric data, which suggest that CO_2 is the dominant volatile species.

The results for individual samples are fairly consistent (Table 5 and Fig. 17). Type 2 and type 3 fluid inclusions have similar volatile compositions. The average proportions of N_2–CH_4–CO_2 of type 2 and type 3 fluid inclusions are 4.07–0.30–95.63%, and 4.01–0.31–95.68% for 01SW-38; 5.18–0.46–94.36%, and 4.30–0.28–95.42% for 76608; 14.23–0.57–85.19%, and 12.55–0.73–86.71% for GC01-123; and 8.04–0.75–91.21%, and 9.23–1.14–89.63% for GC01-69 (Table 5).

Pressure Estimation

Because fluid inclusions in the chlorite-calcite alteration stage are aqueous inclusions that homogenize into the liquid phase (Th = 116° to 159°C), the trapping temperature and pressure cannot be independently determined. In the sericite–ankerite alteration assemblage, the occurrence of types 1, 2a, 2b, and 3 fluid inclusions is interpreted to reflect the involvement of two fluids (one represented by type 1 and the other by type 3 inclusions) from different sources, which mixed at the site of mineralization in variable proportions to form type 2 inclusions. Some of the type 2 inclusions might have been saturated with carbonic components at entrapment and so their homogenization temperatures represent the trapping temperatures. The homogenization temperatures of the majority of type 2 inclusions, mainly between 220° and 270°C (Fig. 16D), are likely close to the fluid temperatures at the mineralization stage. Fluid pressures are estimated based on the isochores of the type 3 fluid inclusions, which are approximated by the system CO_2–N_2–CH_4, because the proportion of the aqueous phase is too small to be measured. For a sample that has laser Raman data, the composition is approximated by the average CO_2–N_2–CH_4 values of type 3 fluid inclusions of that sample. For the other samples, the average values of the whole sample set (Table 2) are used. The isochores (Fig. 18) were constructed using the equation of state of Holloway (1981). Using the 220° to 270°C range as the temperature of mineralization, the fluid pres-

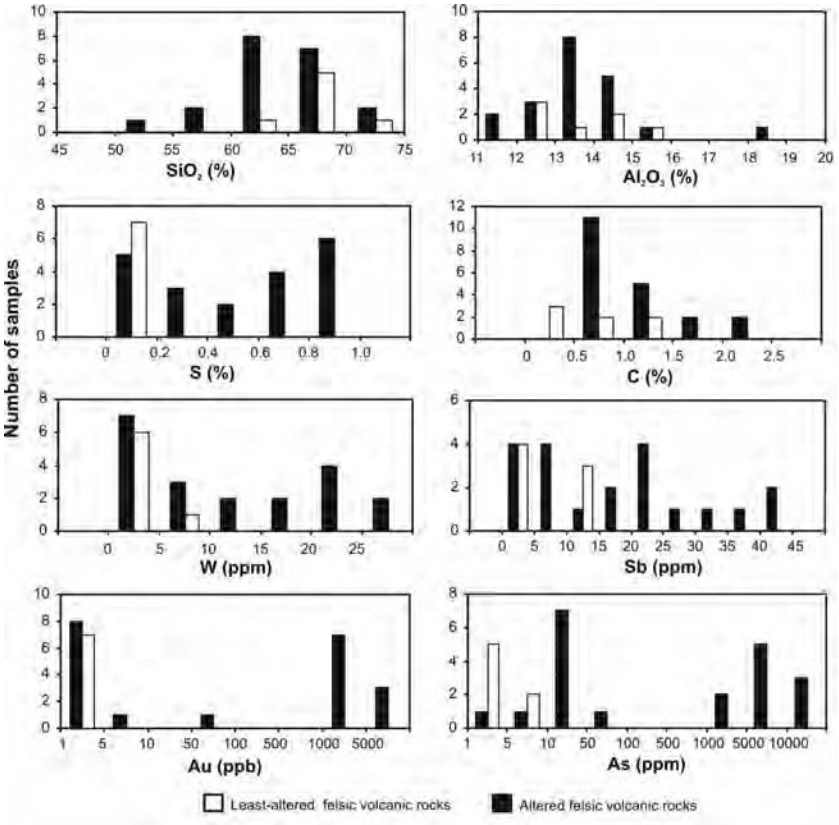

Fig. 12. Histograms of major and trace element compositions of least-altered and altered felsic volcanic rocks from the study area.

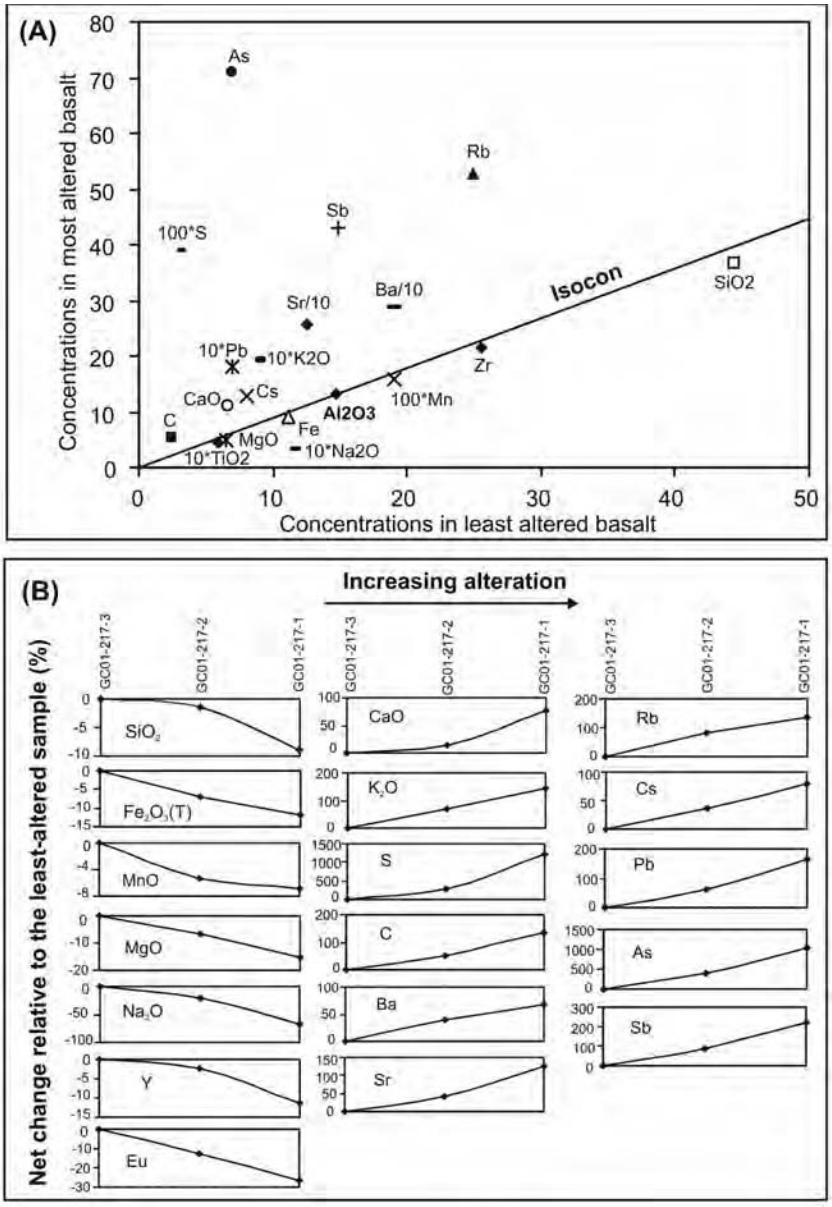

Fig. 13. ***A***. An isocon graph illustrating the gain and loss of different elements in a pair of least-altered and most-altered basalts. The isocon is based on aluminum immobility. Units are wt.% for major elements and ppm for trace elements. ***B***. Net changes of components and elements relative to the least-altered sample (in weight percent) for a set of three samples showing progressively increasing degree of alteration (samples GC01-127-3, -2, -1). Negative and positive values indicate net loss and net gain, respectively.

sures are estimated to range from 770 to 1240 bars. Assuming a lithostatic load with a rock density of 2.7 g/cm^3, the depth of mineralization is estimated at 2.9 to 4.6 km. This range of depth is comparable to that of most intrusion-related gold deposits (Lang et al., 2000), and partly overlaps the upper part of greenstone gold deposits (Poulsen et al., 2000).

Carbonate Stable Isotopes

As described above, calcite is associated with chlorite alteration that predates gold mineralization, whereas ankerite is associated with sericite alteration that is synchronous with Au mineralization. The carbon and oxygen isotope compositions were determined for calcite and ankerite. For carbonates disseminated in host rocks, a subset of the powder for major and trace element analyses was treated with different acids such that CO_2 was extracted from calcite and ankerite separately. For carbonates in the veins, separate calcite and ankerite were sampled with a microdrill. In one vein sample (01SW38), calcite and ankerite could not be completely separated with microdrilling, and chemical separation was used as for the disseminated samples.

The results of C and O isotopic analysis are listed in Table 6 and graphically presented in Fig. 19A. The $\delta^{18}O_{SMOW}$ and $\delta^{13}C_{PDB}$ values of premineralization calcite range from +12.7‰ to +17.6‰, and –4.1‰ to –8.0‰, respectively. The $\delta^{18}O_{SMOW}$ and $\delta^{13}C_{PDB}$ values of mineralization-related ankerite range from +14.5‰ to +16.5‰, and –6.8‰ to –8.3‰, respectively. Calcite and ankerite show similar C and O isotopes, but ankerite has a narrower range than calcite (Fig. 19A). Using a temperature of 140ºC for calcite and 250ºC for ankerite, the $\delta^{18}O_{SMOW}$ values of the fluids in equilibrium with calcite and ankerite are calculated to be –2.1‰ to 3.3‰, and 6.4‰ to 8.3‰, respectively (calculated using the equations of Zheng, 1999; Table 6). The C isotopic compositions of the fluids are approximated by those of the minerals because the degree of fractionation is small. The $\delta^{18}O$ and $\delta^{13}C$ values of the fluids are plotted in Fig. 19B. All the fluids in equilibrium with ankerite plot in the field of magmatic water (Sheppard, 1986; Taylor, 1986), whereas all the fluids in equilibrium with calcite plot to the left of the magmatic field (Fig. 19B), indicating meteoric water input. However, it should be noted that the oxygen and carbon isotopes of the fluids associated with ankerite also fall in the broad range for metamorphic fluids (Fig. 19B).

Discussion and Conclusions

The age of the PMVC has been one of the most important problems hindering the understanding of the geologic setting and environment of gold mineralization in this area.

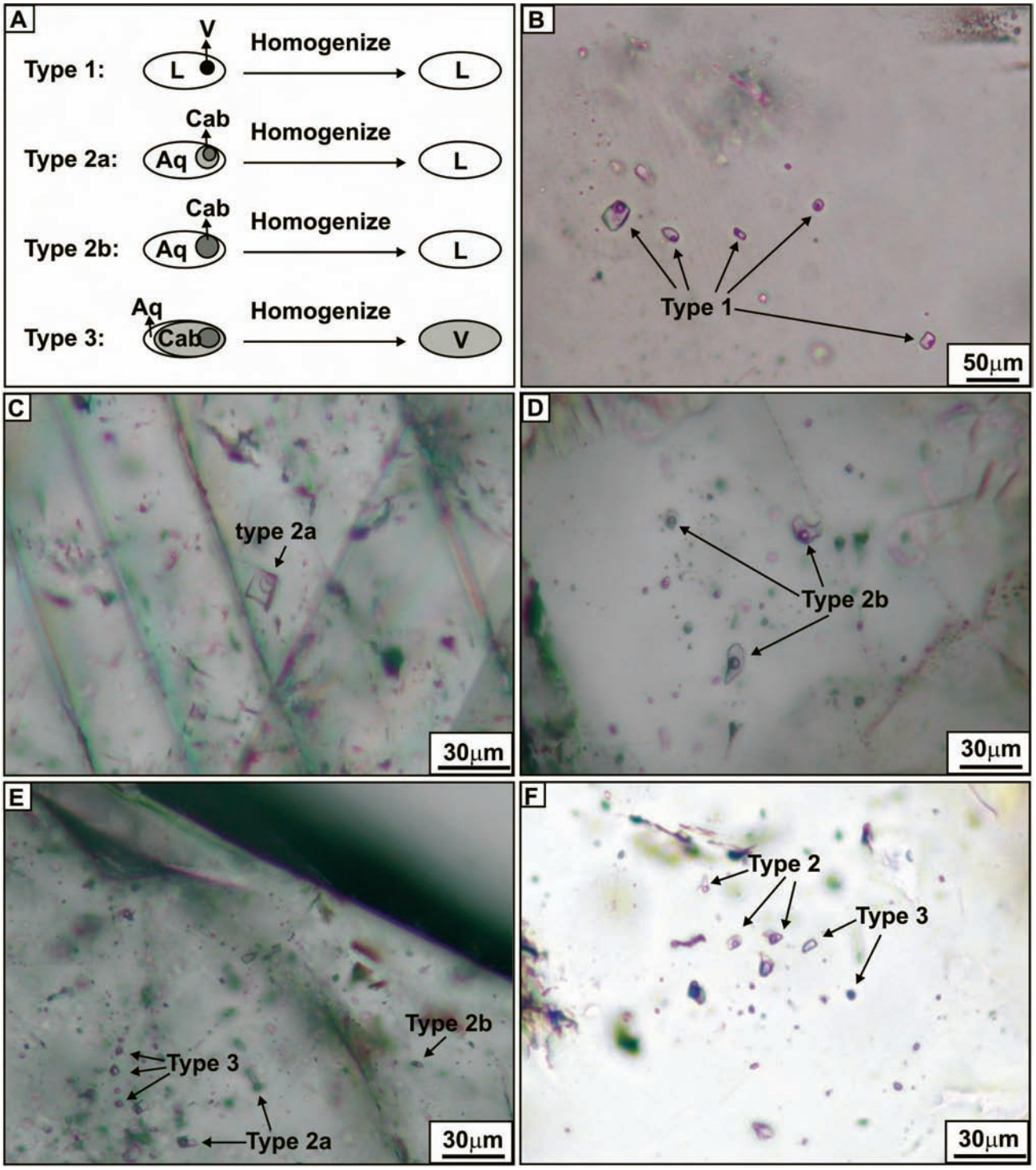

Fig. 14. Types and modes of occurrence of fluid inclusions. ***A***. Schematic representation of fluid inclusion types. ***B***. Cluster of aqueous (type 1) fluid inclusions in premineralization quartz; note consistent vapor ratios (sample 01SW-23). ***C***. Isolated aqueous-carbonic (type 2a) fluid inclusion in ankerite (sample GC01-63). ***D***. Cluster of aqueous-carbonic (type 2b) fluid inclusions in mineralization-stage quartz; note consistent liquid:vapor ratios (sample 01SW-38). ***E***. Short trail of carbonic-aqueous (type 3) fluid inclusions in mineralization-stage quartz; the aqueous phase is not visible; some type 2a and 2b inclusions also occur in the same crystal (sample 76608). The different types of inclusions were not entrapped at the same time: type 3 here might be secondary or pseudosecondary, and type 2 might be primary. ***F***. Cluster of type 2 and 3 inclusions; the variation of liquid:vapor ratios might have resulted from necking (sample GC01-123).

Its proximity to the Ordovician Meductic Group and the Early Devonian Tobique Group volcanic rocks (Fig. 1) has made it tempting to assign the PMVC to one or other of these groups. In the regional tectonic framework, the Me-

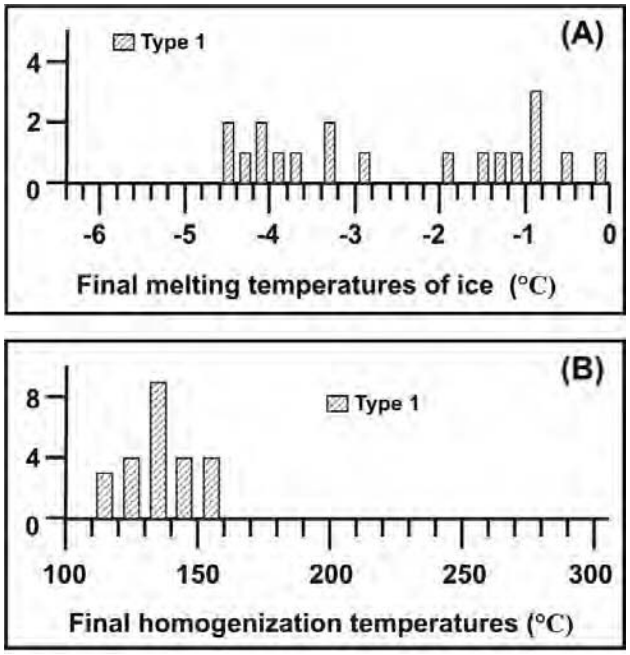

Fig. 15. Microthermometric data of fluid inclusions from premineralization calcite and quartz: ***A***. Histogram of final melting temperatures of ice; ***B***. Histogram of final homogenization temperatures.

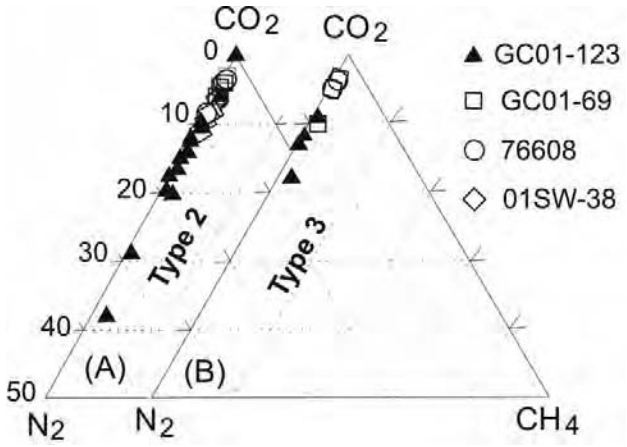

Fig. 17. Volatile composition of the vapor phase of fluid inclusions analyzed by laser Raman spectroscopy (mole %): ***A*** Type 2 fluid inclusions. ***B***. Type 3 fluid inclusions.

ductic Group volcanic rocks were formed on the continental margin in relation to the SE-directed subduction of the Iapetus Ocean in the Early Ordovician (Fyffe, 2001), whereas the Devonian rocks were formed after the Late Ordovician to Late Silurian closure of the Iapetus Ocean (van Staal, 1994). The majority of zircon recovered from the PMVC porphyritic felsic volcanic rock have ages of ca. 460 Ma. However, the diversity of the zircon population is interpreted to be due to inheritance, and thus only a maximum age of 460 Ma is established for the intrusion. These data indicate that the PMVC is younger than the Meductic Group, which must be older than 479 ± 7 Ma (the age of the Benton granodiorite that intrudes the Meductic Group; Whalen et al., 1998). A minimum age for the PMVC is provided by the 411 ± 3.7 Ma Ar–Ar age of the sericite that cuts the PMVC rock. Two zircon grains with ca. 390 Ma U–Pb ages are younger than the Ar–Ar age determined for crosscutting sericite. Interpretation of these two zircon

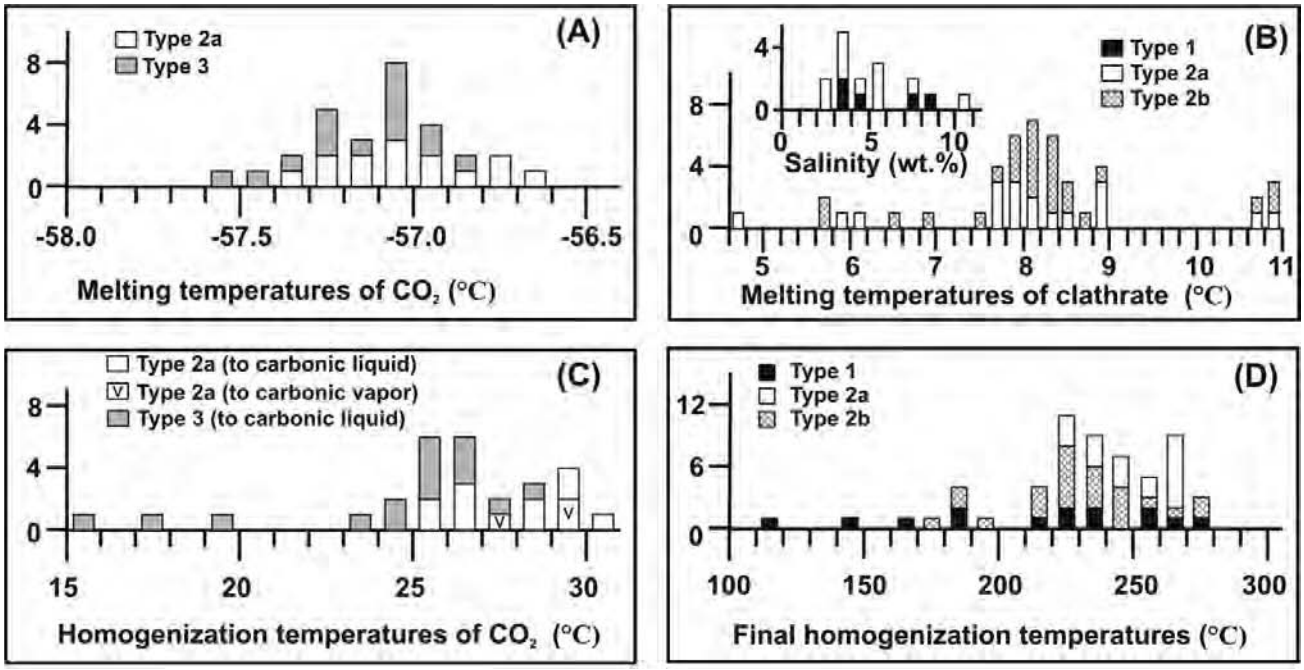

Fig. 16. Microthermometric data of fluid inclusions from mineralization-stage quartz and ankerite: ***A***. Histogram of melting temperatures of CO_2; ***B***. Histogram of melting temperatures of clathrate and salinities (wt.% NaCl equiv.); ***C***. Histogram of homogenization temperatures of CO_2; ***D***. Histogram of final homogenization temperatures.

Table 4. Fluid Inclusion Microthermometric Data

Sample	Host Mineral	Occur.	Size (μm)	V/T (%)	Type	Tm_{CO2}(°C) Mean (*n*)	Tm_{H2O}(°C) Mean (*n*)	Tm_{clath}(°C) Mean (*n*)	Th_{CO2} (°C) Range	Th_{CO2} (°C) Mean (*n*)	Salinity Mean (*n*)	Th (°C) Range	Th (°C) Mean (*n*)
GC01–140	Calcite (pre–ore vein)	Cluster	5–15	10	1	–	–1.8	–	–	–	3.1	126–134	130 (2)
		Isolated	10	10	1	–	–0.1	–	–	–	0.2	123	123
		Isolated	17	10	1	–	–0.4	–	–	–	0.7	137	137
		Isolated	12	10	1	–	–0.8	–	–	–	1.4	116	116
		Cluster	10	10	1	–	–0.8	–	–	–	1.4	120	120
		Cluster	6–16	10	1	–	–1.0 (2)	–	–	–	1.7 (2)	117–120	118 (3)
GC01–40	Calcite (pre–ore, replacing phenos)	Cluster	8–12	10	1	–	–4.3 (2)	–	–	–	6.9 (2)	132–135	134 (3)
		Cluster	5–14	10	1	–	–3.2	–	–	–	5.3	129–140	136 (5)
		Cluster	5–10	10	1	–	–4.5 (2)	–	–	–	7.2 (2)	132–136	134 (4)
		Cluster	4–6	10	1	–	–4.5	–	–	–	7.2	128–135	132 (2)
		Cluster	3–10	10	1	–	–4.1	–	–	–	6.6	129–135	132 (3)
		Isolated	10	10	1	–	–4.1	–	–	–	6.6	128	128
		Isolated	3–10	10	1	–	–	–	–	–	–	133	133
GC01–135	Calcite (amigd.)	Isolated	10	10	1	–	–2.8	–	–	–	4.6	152	152
		Isolated	8	10	1	–	–3.3	–	–	–	5.4	147	147
01SW23	Quartz (pre–ore vein, assoc cal)	Cluster	6–8	10	1	–	–1.3 (2)	–	–	–	2.2 (2)	151–158	155 (3)
		Cluster	5–12	10	1	–	–1.5 (2)	–	–	–	2.6 (2)	151–164	159 (4)
		Isolated	6	10	1	–	–	–	–	–	–	139	139
		Isolated	6	10	1	–	–	–	–	–	–	147	147
		Isolated	15	10	1	–	–0.9	–	–	–	1.6	143	143
GC01–71	Calcite (pre–ore, assoc, Py)	Isolated	10	10	1	–	–3.8	–	–	–	6.2	153	153
		Isolated	5	10	1	–	–	–	–	–	–	127	127
		Isolated	8	10	1	–	–	–	–	–	–	122	122
		Isolated	10	10	1	–	–3.7	–	–	–	6.0	148	148
	Quartz (ore stage)	Cluster	5–7	10	1	–	–4.8	–	–	–	7.6	161–170	165 (2)
		Cluster	6–7	10	1	–	–5.2	–	–	–	8.1	179–187	183 (2)
GC01–69	Quartz (vein assoc arsenopyrite)	Isolated	7	20	1	–	–	–	–	–	–	257	257
		Cluster	6–7	20	2a	–57.1	–2.8	8.8 (2)	–	–	–	261–274	268 (2)
		Isolated	8	25	2a	–57.2	–	8.8	25.1 L	25.1	2.3	266	266
		Random	6–12	20	2a	–57.0 (2)	–3.4	8.8 (4)	29.8–29.8 V	29.8 (2)	2.3 (2)	239–266	251 (4)
		Random	7–11	20	2a	–56.6	–3.4	8.2 (2)	29.4–30.0 V	29.7 (2)	3.7 (2)	231–241	235 (3)
		Random	10–14	15	2a	–56.7 (2)	–2.8	8.4 (2)	29.0–29.4 L	29.2 (2)	3.2 (2)	203–242	221 (3)
		Short trail	5–7	100	3	–57.5 (3)	–	–	11.4–20.9 L	15.9 (3)	–	–	–
		Cluster	6–8	100	3	–57.4 (2)	–	–	23.9–26.3 L	25.1 (2)	–	–	–
		Cluster	5–8	100	3	–57.2 (2)	–	–	24.3–24.4 L	24.4 (3)	–	–	–
GC01–123	Quartz (cement in breccia assoc. with arsenopyrite)	Isolated	8	15	1	–	–	–	–	–	–	222	222
		Isolated	8	15	1	–	–	–	–	–	–	231	231
		Random	9–9	10	1	–	–2.0 (2)	–	–	–	3.4 (2)	139–157	148 (2)
		Isolated	10	15	2a	–56.8	–5.0	8.1	–	–	–	242	242
		Random	12	20	2a	–57.2	–5.1	8.0	25.5 L	25.5	3.1	263	263
		Isolated	10	10	2a	–56.9	–5.1	7.6	–	–	–	247	247
		Isolated	10	10	2a	57.0	–5.2	7.8	–	–	–	238	238
		Isolated	12	25	2a	–56.9	–	6.0	–	–	–	252	252
		Cluster	10–11	25	2a	–57.1 (2)	–4.2	5.8	27.8–28.0 V	27.9 (2)	7.8	269–271	270 (2)
		Isolated	7	15	2b	–	–3.4	8.4	–	–	–	220	220
		Isolated	7	15	2b	–	–3.5	8.7	–	–	–	249	249
		Cluster	5–9	15	2b	–	–4.7	7.4	–	–	–	217–242	229 (2)
		Cluster	9	15	2b	–	–5.2	6.8	–	–	–	188	187
		Random	7–10	15	2b	–	–5.3	6.4	–	–	–	240–243	241 (2)
		Cluster	4–8	100	3	–57.3 (2)	–	–	14.9–20.1 L	17.5 (4)	–	–	–
		Random	4–8	100	3	–57.2 (2)	–	–	18.5–20.9 L	19.2 (5)	–	–	–

Table 4. (Continued)

Sample	Host Mineral	Occur.	Size (μm)	V/T (%)	Type	Tm_{CO2}(°C) Mean (*n*)	Tm_{H2O}(°C) Mean (*n*)	Tm_{clath}(°C) Mean (*n*)	Th_{CO2} (°C) Range	Th_{CO2} (°C) Mean (*n*)	Salinity Mean (*n*)	Th (°C) Range	Th (°C) Mean (*n*)
GC01–63	Quartz (vein assoc. arsen–Ankerite)	Random	5–7	10	1	–	–1.8 (2)	–	–	–	3.1 (2)	108–119	113 (4)
		Isolated	6	30	1	–	–	–	–	–	–	234	234
		Random	6–9	30	2a	–57.2 (7)	–3.5	7.6 (5)	26.0–27.0 L	26.5 (7)	4.6 (5)	247–287	262 (7)
		Isolated	12	30	2a	–57.2	–	10.6	29.6 L	29.6	–	249	249
		Isolated	20	15	2a	–57.3	–2.4	10.8	30.2 L	30.2	–	235	235
		Cluster	6–7	25	2b	–	–5.4	8.3 (2)	–	–	–	264–269	266 (2)
		Isolated	7	25	2b	–	–	8.4	–	–	–	250	250
		Isolated	6	30	2b	–	–	10.8	–	–	–	235	235
		Isolated	8	30	2b	–	–	10.8	–	–	–	232	232
		Isolated	7	25	2b	–	–	10.6	–	–	–	238	238
		Isolated	7	20	2b	–	–	8.1	–	–	–	238	238
		Isolated	7	25	2b	–	–	8.8	–	–	–	222	222
		Cluster	5–8	25	2b	–	–	8.3 (2)	–	–	–	198–217	212 (2)
		Isolated	10	100	3	–57.0	–	–	25.0 L	25.0	–	–	–
		Isolated	9	100	3	–57.0	–	–	25.1 L	25.1	–	–	–
97SW–46	Quartz (vein assoc. arsenopyrite)	Isolated	4	15	1	–	–	–	–	–	–	267	267
		Isolated	4	15	1	–	–	–	–	–	–	220	220
		Isolated	9	10	1	–	–	–	–	–	–	253	253
		Isolated	6	25	1	–	–	–	–	–	–	273	273
		Cluster	6–7	15	2b	–	–5.6 (2)	7.8	–	–	–	213–228	220 (2)
		Isolated	5	20	2b	–	–5.5	8.1	–	–	–	277	277
		Isolated	6	20	2b	–	–	8.3	–	–	–	246	246
		Cluster	6	20	2b	–	–	8.0	–	–	–	279	279
		Cluster	6	20	2b	–	–	8.3	–	–	–	244	244
		Cluster	7	85	3	–57.2	–	–	26.1 L	26.1	–	293 V	293
		Cluster	5	100	3	–57.1	–	–	25.9 L	25.9	–	–	–
01SW38	Quartz (vein assoc. ankerite)	Cluster	8–13	25	2a	–57.3 (3)	–	7.6	28.2–28.6 L	28.4 (3)	5.6	250–266	260 (4)
		Short trail	9–13	25	2a	–57.0	–	7.8	26.6–27.0 L	26.8 (2)	5.3	219–232	227 (3)
		Isolated	10	30	2a	–56.7	–	4.6	28.6 L	28.6	10.6	264	264
		Isolated	8	20	2a	–57.2	–	7.8	26.3 L	26.3	5.3	223	223
		Cluster	8–11	25	2b	–	–4.5	7.7	–	–	–	202–222	212 (4)
		Short trail	12–15	20	2b	–	–2.9	8.1	–	–	–	182–202	192 (2)
		Isolated	8	20	2b	–	–	5.6	–	–	–	237	237
		Isolated	13	25	2b	–	–	5.6	–	–	–	227	227
		Isolated	6	20	2b	–	–	7.8	–	–	–	228	228
		Short trail	6–8	15	2b	–	–4.8	7.8 (2)	–	–	–	201–225	215 (4)
		Cluster	6–7	100	3	–57.0	–	–	27.9–28.3 L	28.1 (2)	–	–	–
		Isolated	6	100	3	–56.8	–	–	23.5 L	23.5	–	–	–
		Short trail	6–9	100	3	–56.9	–	–	22.0–25.1 L	24.1 (4)	–	–	–
		Short trail	6–12	100	3	–57.0	–	–	24.9–27.3 L	26.4 (3)	–	–	–
76608	Quartz (vein assoc. arsenopyrite)	Isolated	6	20	1	–	–2.5	–	–	–	4.2	188	188
		Isolated	5	20	1	–	–	–	–	–	–	212	212
		Isolated	6	20	2b	–	–3.0	8.2	–	–	–	186	186
		Isolated	6	20	2b	–	–	8.1	–	–	–	175	175
		Short trail	2–5	100	3	–56.9	–	–	26.2–26.4 L	26.3 (3)	–	–	–
		Short trail	4–8	100	3	–57.0	–	–	27.2–27.3 L	27.3 (2)	–	–	–

Notes

Abbreviations: Tm_{CO2} = melting temperature of CO_2; Tm_{H2O} = melting temperature of ice; Tm_{clath} = melting temperature of clathrate; Th_{CO2} = homogenization temperature of CO_2; Th = total homogenization temperature; V/T = vapor/total inclusion volume ratio; – = not analyzed.

Salinity in wt.% NaCl equivalent. Type 1 is approximated by H_2O-NaCl system, and type 2 by H_2O-CO_2-N_2-NaCl system using the equations of Soave (1972) in the program "Clathrates" by Bakker (1997).

Table 5. Volatile Composition of the Vapor Phase of Fluid Inclusions

Sample	FI Type	N_2 (mol%)	CH_4 (mol%)	CO_2 (mol%)
01SW-38-1	2	4.44	0.24	95.32
01SW-38-2	2	3.50	0.43	96.06
01SW-38-3	2	2.59	0.28	97.13
01SW-38-4	2	5.75	0.23	94.02
01SW-38-5	3	3.08	0.34	96.58
01SW-38-6	3	4.94	0.27	94.79
Average 01SW-38 type 2	2	4.07	0.30	95.63
Average 01SW-38 type 3	3	4.01	0.31	95.68
76608-1	2	8.13	0.25	91.62
76608-2	2	3.84	0.29	95.87
76608-3	2	3.09	0.50	96.41
76608-4	2	5.67	0.79	93.54
76608-5	3	4.96	0.26	94.78
76608-6	3	3.64	0.30	96.06
Average 76608 type 2	2	5.18	0.46	94.36
Average 76608 type 3	3	4.30	0.28	95.42
GC01-123a1	2	18.96	0.63	80.40
GC01-123a2	2	13.49	0.56	85.96
GC01-123a3	2	11.78	0.16	88.07
GC01-123a4	2	9.52	0.16	90.32
GC01-123a5	2	15.99	0.62	83.40
GC01-123b1	2	12.27	0.22	87.51
GC01-123b2	2	7.63	0.62	91.76
GC01-123b3	2	5.18	0.77	94.04
GC01-123b4	2	10.05	0.48	89.46
GC01-123c1	2	17.76	0.00	82.24
GC01-123c2	2	28.27	0.69	71.04
GC01-123c3	2	7.17	0.70	92.13
GC01-123d1	2	0.00	0.00	100.00
GC01-123d2	2	15.00	0.00	85.00
GC01-123d3	2	18.62	1.69	79.69
GC01-123d4	2	36.06	1.88	62.05
GC01-123a6	3	12.97	0.28	86.75
GC01-123b5	3	8.89	0.69	90.42
GC01-123c4	3	11.76	0.18	88.06
GC01-123d5	3	16.60	1.79	81.61
Average GC01-123 type 2	2	14.23	0.58	85.19
Average GC01-123 type 3	3	12.55	0.73	86.72
G01-69a	2	5.91	0.73	93.36
G01-69b	2	8.03	0.49	91.48
G01-69c	2	8.83	0.73	90.44
G01-69d	2	10.29	0.76	88.94
G01-69e	2	7.16	1.01	91.83
G01-69f	3	9.23	1.14	89.63
Average GC01-69 type 2	2	8.04	0.75	91.21
Average GC01-69 type 3	3	9.23	1.14	89.63

Notes
Abbreviations: FI = fluid inclusion.
Analyzed by laser Raman spectroscopy.

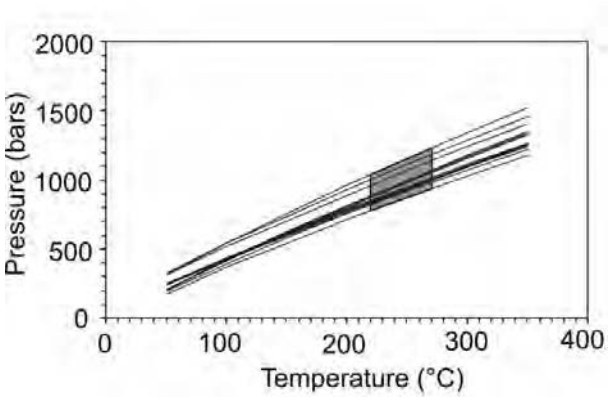

Fig. 18. Isochores of type 3 fluid inclusions. The shaded area indicates the possible range of temperature and pressure of the mineralizing fluids.

ages is difficult because they represent a small proportion of the zircon recovered. Although every effort has been made to avoid contamination during sample collection and preparation, this is considered the best explanation for the two young grains. The best age estimate for the PMVC is therefore interpreted to be between 411 ± 3.7 Ma and 459 ± 3 Ma. The PMVC might have been formed during the Middle to Late Ordovician back-arc volcanism, or during the closure of the Iapetus Ocean from the Late Ordovician to Late Silurian (van Staal, 1994)

Considering the regional and local geological settings, three hypotheses for the genesis of gold mineralization at Poplar Mountain are possible: (1) the mineralization was genetically related to the PMVC; (2) it was associated with hydrothermal fluids ascending from depth and focused along the Woodstock fault; or (3) it was related to fluids emanating from unexposed Devonian granitic intrusions.

The first hypothesis implies a relatively shallow depth of mineralization, and that the formation of the host rocks and mineralization was coeval. This hypothesis is superficially supported by the style of deformation (dominantly brittle) and the widespread chlorite–calcite–quartz alteration, which might be compared to propylitization in epithermal-type deposits, or the outer zones of porphyry-type systems. The fluid inclusion data document two hydrothermal events in the PMVC. The first is related to the chlorite–calcite–quartz alteration, and the second is related to sericite–ankerite–quartz alteration (plus gold mineralization). Fluids of the first hydrothermal event (salinities of 0.2–7.1 wt.% NaCl equivalent; homogenization temperatures of 116° to 159°C) are broadly compatible with an epithermal system (Cooke and Simmons, 2000), but this hydrothermal event is not related to gold mineralization based on petrographic and paragenetic studies. As discussed above, the mineralization might have been younger than the host rocks, but the possibility that it is broadly coeval with the host rocks cannot be ruled out. However, fluid inclusion data indicate that during mineralization, fluid pressures were fairly high and corresponded to lithostatic depths of 2.9 to 4.6 km, whereas the host rocks were formed on the surface (volcaniclastic rocks and basalt) or near surface (porphyritic felsic volcanic rock). Therefore,

Table 6. Oxygen and Carbon Isotopes of Carbonates and Calculated Oxygen Isotopic Compositions of Fluids

	Calcite		$Fluid_{equilb.\ Cal.}$	Ankerite		$Fluid_{equilb.\ Ank.}$
Sample	**$\delta^{18}O$ (‰, SMOW)**	**$\delta^{13}C$ (‰, PDB)**	**$\delta^{18}O$ (‰, SMOW) (T = 140˚C)**	**$\delta^{18}O$ (‰, SMOW)**	**$\delta^{13}C$ (‰, PDB)**	**$\delta^{18}O$ (‰, SMOW) (T = 250˚C)**
Carbonates disseminated in host rocks						
GC01–127–1	17.4	–7.5	3.0	16.0	–7.7	7.8
GC01–127–2	16.9	–7.1	2.6	14.6	–7.4	6.4
GC01–127–3	16.0	–7.1	1.7	15.6	–6.8	7.4
GC01–138	15.4	–8.0	1.1	16.5	–7.1	8.3
01SW15	15.2	–6.6	0.9	16.1	–7.1	7.9
01SW46–1	15.1	–7.0	0.8	15.6	–7.1	7.5
GC01–79	15.3	–7.0	0.9			
GC01–80	12.7	–5.5	–1.6	14.5	–7.3	6.4
GC01–81	12.3	–7.7	–2.1	14.6	–7.3	6.5
GC01–77	17.6	–7.4	3.3	16.0	–7.6	7.9
GC01–47	16.8	–7.3	2.4	15.8	–7.7	7.7
Carbonates in veins						
GC01–74	15.6	–5.2	1.3	–	–	–
GC01–60	14.9	–7.0	0.5	–	–	–
01SW38–b	15.3	–7.4	1.0	–	–	–
01SW23	15.8	–4.1	1.5	–	–	–
01SW38–a	–	–	–	15.3	–8.3	7.1
01SW32	–	–	–	15.6	–6.8	7.4

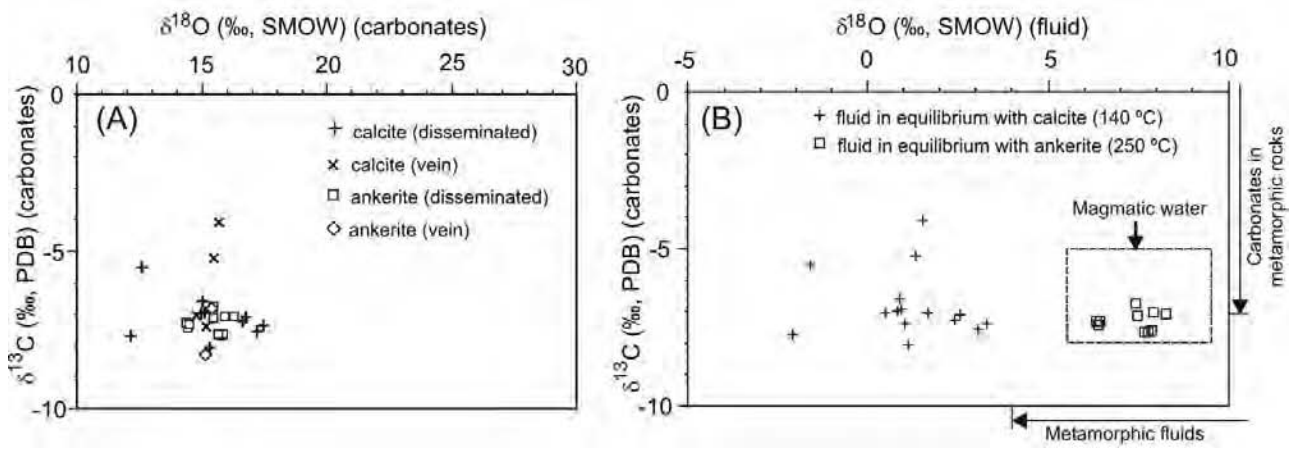

Fig. 19. ***A***. Carbon and oxygen isotopes of calcite and ankerite. ***B***. Carbon isotopes of calcite and ankerite and oxygen isotopes of the fluids in equilibrium with calcite and ankerite (Table 2). The range for magmatic fluids is from Sheppard (1986) and Taylor (1986). The range of oxygen isotopes of metamorphic fluids is from Sheppard (1986), and the range of carbon isotopes of carbonates in metamorphic rocks are from Valley (1986).

if the mineralization is genetically related to the PMVC, it must have taken place after the host rocks had been buried to significant depth by continual volcanic activity, with ore-forming fluids being provided or driven by co-genetic, relatively deep-seated intrusions.

The second and third hypotheses are not mutually exclusive, except that the third hypothesis specifies that the ore-forming fluids were derived from granitic intrusions. The type of alteration associated with mineralization (ankerite–sericite) and the composition of the ore-forming fluids (CO_2-rich) are common in mesothermal or orogenic-type gold deposits (Ridley and Diamond, 2000; Groves et al., 2003). Mesothermal gold deposits are generally spatially controlled by structures, and their ore-forming fluids have variously been attributed to magmatic, metamorphic, or meteoric origin, as discussed in Kerrich (1989). Although there is no consensus on the source of most mesothermal gold deposits (in particular magmatic versus metamorphic origin; e.g., Groves et al., 2003), some are apparently related to granitic intrusions (Thompson and Newberry, 2000; Lang and Baker, 2001; Baker, 2002; Groves et al., 2003). A magmatic origin (Fig. 20) is favored for the ore-forming fluids of Poplar Mountain based on the following five observations. First, the Poplar Mountain gold occurrence is only 8 km from the surface exposure of the northwestern edge of the Pokiok batholith, and gold mineralization of

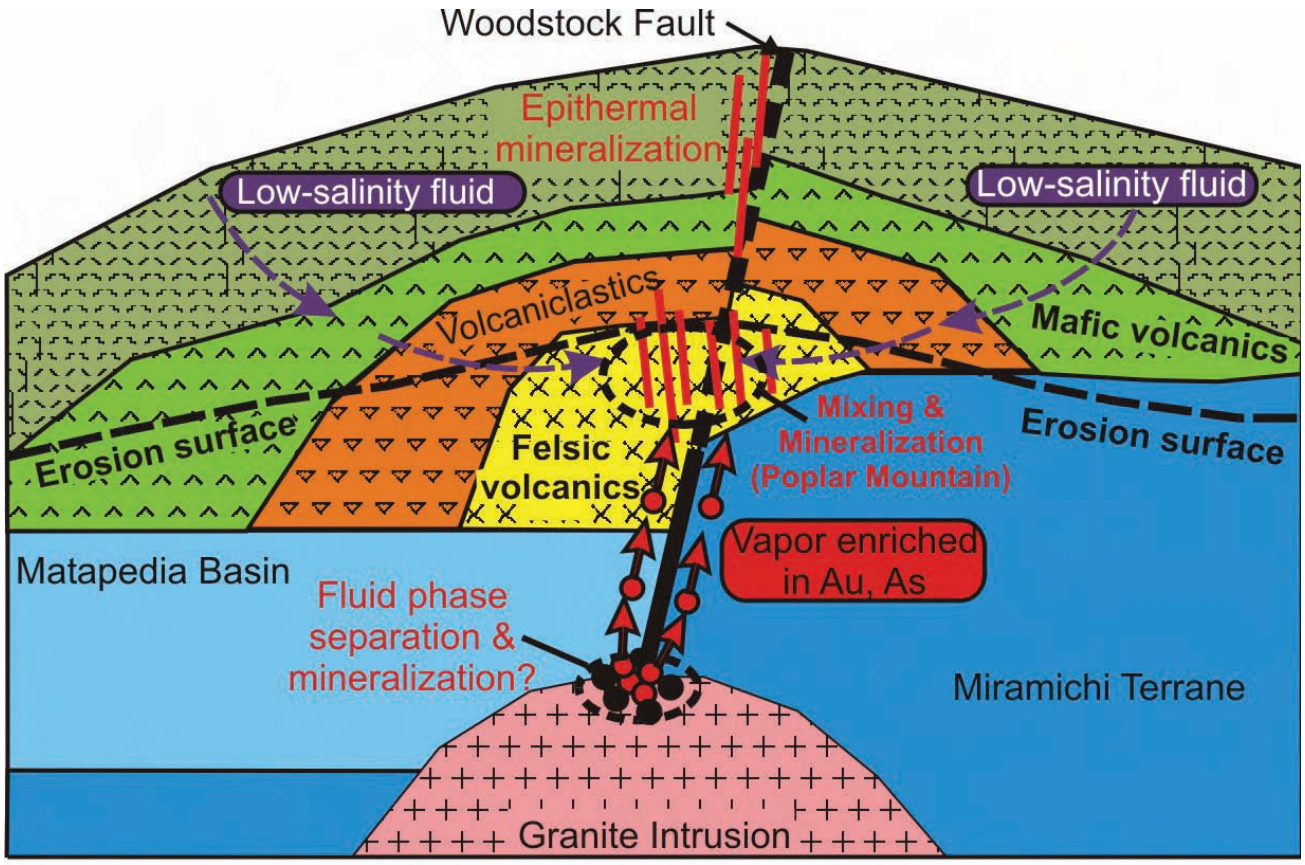

Fig. 20. A schematic genetic model of the Poplar Mountain gold occurrence. Gold mineralization is related to a hidden granitic intrusion, from which an Au-, As-, and carbonic-enriched fluid was derived from phase separation. This magmatic fluid ascended along the Woodstock fault, mixed with a low-salinity, low-temperature fluid, and precipitate arsenopyrite and gold at Poplar Mountain.

the same age has been documented associated with an unexposed intrusion near the southeastern edge of the batholith (Lake George; Yang et al., 2002). Second, the age of mineralization (411 ± 3.7 Ma, based on $^{40}Ar/^{39}Ar$ dating of sericite) is broadly contemporaneous with the Pokiok batholith (402–415 Ma), and is similar to the age of gold mineralization at Lake George (ca. 410 Ma, $^{40}Ar/^{39}Ar$ method). Third, magnetic data suggest that the PMVC is underlain by a granitic intrusion (Freewest Resources Canada Inc., unpub. report, 1999). Fourth, mineralization-associated alteration is accompanied by enrichment of K, Rb, Cs, Ca, Sr, Ba, As, Sb, W, C, and S, many of which are granophile elements, although these elements are also characteristic of mesothermal gold deposits without obvious magmatic association (Kerrich, 1989). Finally, the carbon and oxygen isotopic signatures of the fluids associated with sericite–ankerite–quartz alteration and mineralization fall well within the magmatic range, although they are also in the range of metamorphic fluids. It should be pointed out that none of the above observations alone is a sufficient indicator of a magmatic origin. Thus, the possibility of the ore-forming fluids being of metamorphic origin, focused along the Woodstock fault, cannot be ruled out. Our inclination toward a magmatic origin is partly based on consideration of the regional geologic setting, i.e., a region characterized by extensive granitic intrusions with related W-Sn-Mo-Sb mineralization.

The fluid inclusion study indicates that two immiscible fluids (an aqueous liquid and a carbonic vapor) were involved in the mineralization at Poplar Mountain. Using the phase relationships of the $NaCl–H_2O–CO_2$ system (Duan et al., 1995) as an approximation for the Poplar Mountain mineralizing fluids, it can be shown that the two immiscible fluids could not have resulted from in situ unmixing at the temperature conditions (<280°C). In other words, if the two immiscible fluids originated from unmixing of an originally homogeneous fluid, then the unmixing process is likely to have taken place at a greater depth, before the fluids ascended to the site of mineralization. This is even more likely if CH_4 and N_2 are taken into account. The two immiscible fluids might both have been derived from this deep-seated unmixing, or one of them (more likely the carbonic-enriched vapor phase) was derived from such unmixing, and the other (aqueous liquid) was from a separate source (e.g., from the country rocks). The lack of base metal enrichment at the Poplar Mountain gold occurrence is likely due to the low salinity of the ore-forming fluids. It has been shown that gold hydrosulfide complexes such as $AuHS(H_2S)_3^0$ play a fundamental role in the formation of the majority of hydrothermal gold deposits (Seward, 1991;

Loucks and Mavrogenes, 1999). It has also been shown that Au, Cu, As, and B have the tendency of being selectively partitioned into the vapor phase, together with H_2S, in a boiling magmatic fluid system, whereas most base metals are enriched in the liquid brine (Heinrich et al., 1999). CO_2-dominated auriferous or copper-rich fluids have been proposed in orogenic-type gold deposits (Schmidt Mumm et al., 1997; Chi et al., 2006) and a skarn-porphyry deposit (Lai and Chi, in review). In the case of Poplar Mountain, we might envisage that the carbonic-enriched vapor phase was derived from unmixing of a magmatic fluid at depth and carried Au and As, which were deposited when a cooler, low-salinity aqueous fluid was met at the site of mineralization (Fig. 20). In addition to temperature drop, the leaching of Fe during alteration (Fig. 13) might have contributed to mineralization by supplying part of the iron for arsenopyrite precipitation.

In conclusion, although the Poplar Mountain gold occurrence is hosted in volcanic and subvolcanic rocks, and some alteration and veining features similar to epithermal systems are preserved, the gold mineralization is similar to mesothermal or orogenic-type gold deposits in terms of alteration (ankerite-sericite) and composition of ore-forming fluids (CO_2-enriched). Petrographic evidence indicates that the mesothermal-style mineralization was superimposed on the epithermal system at a later time. Although geochemical data cannot rule out a metamorphic origin for the ore-forming fluids, it is proposed that they were derived from deep-seated granitic intrusions and focused along the regional-scale Woodstock fault, and that the gold mineralization system at Poplar Mountain is part of a granitic intrusion-related gold system (Fig. 20).

Acknowledgments

This study is financially supported by the Geological Survey of Canada Targeted Geoscience Initiative (TGI) Program. We thank L. Fyffe, M. McLeod, D. Lentz, B. Dubé, A. Tremblay, and X. Yang for helpful discussion during various stages of the study. M. McLeod, D. Lentz and K. Thorne reviewed various drafts of this paper, and provided constructive comments which help improve the quality of the paper. Comments of two reviewers for the Exploration and Mining Geology have improved the clarity of the paper. A detailed final review by Editor J.P. Richards has greatly improved the quality of the paper. Freewest Resources Canada kindly provided access to their properties, core facilities, and reports.

References

Baker, T., 2002, Emplacement depth and carbon dioxide-rich fluid inclusions in intrusion-related gold deposits: Economic Geology, v. 97, p. 1111–1118.

Bakker, R.J., 1997, Clathrates: Computer programs to calculate fluid inclusion V–X properties using clathrate melting temperatures: Computer Geosciences, v. 23, p. 1–18.

Bevier, M.L., and Whalen, J.B., 1990, Tectonic significance of Silurian magmatism in the Canadian Appalachians: Geology, v. 18, p. 411–414.

Bodnar, R.J., 1993, Revised equation and table for determining the freezing point depression of H_2O-NaCl solutions: Geochimica et Cosmochimica Acta, v. 57, p. 683–684.

Bourque, P.-A., Brisbois, D., and Malo, M., 1995, Gaspé belt, *in* Williams, H., ed., Chapter 4, Geology of the Appalachian-Caledonian orogen in Canada and Greenland: Geological Survey of Canada, Geology of Canada, no. 6, p. 316–351.

Chi, G., 2002, Fluid compositions and temperature-pressure conditions of intrusion-related gold systems in southwestern New Brunswick—A fluid inclusion study: Geological Survey of Canada, Current Research, 2002-E13, 11 p.

Chi, G., and Watters, S., 2002, The Poplar Mountain Au occurrence, southwestern New Brunswick—A preliminary geologic and petrographic study: Geological Survey of Canada, Current Research 2002-D6, 11 p.

Chi, G., Dubé, B., Williamson, K., Williams-Jones, A.E., 2006, Formation of the Campbell-Red Lake gold deposit by H_2O-poor, CO_2-dominated fluids: Mineralium Deposita, v. 40, p. 726–741.

Cooke, D.R., and Simmons, S.F., 2000, Characteristics and genesis of epithermal gold deposits, *in* Hagemann, S.G., and Brown, P.E., eds., Gold in 2000: Reviews in Economic Geology, v. 13, p. 221–244.

Cumming, G.L., and Richards, J.R., 1975, Ore lead in a continuously changing Earth: Earth and Planetary Science Letters, v. 28, p. 155–171.

Duan, Z., Moller, N., and Weare, J.H., 1995, Equation of state for the NaCl-H_2O-CO_2 system: Prediction of phase equilibria and volumetric properties: Geochimica et Cosmochimica Acta, v. 59, p. 2869–2882.

Evensen, N.M., Hamilton, P.J., and O'Nions, R.K., 1978, Rare-earth abundances in chondritic meteorites: Geochimica et Cosmochimica Acta, v. 42, p. 1199–1212.

Fyffe, L.R., 2001, Stratigraphy and geochemistry of Ordovician volcanic rocks of the Eel River area, west-central New Brunswick: Atlantic Geology, v. 37, p. 91–103.

Grant, J.A., 1986, The isocon diagram—A simple solution to Gresens' equation for metasomatic alteration: Economic Geology, v. 81, p. 1976–1982.

Gresens, R.L., 1967, Composition-volume relationships of metasomatism: Chemical Geology, v. 2, p. 47–55.

Groves, D.I., Goldfarb, R.J., Robert, F., and Hart, G.J.R., 2003, Gold deposits in metamorphic belts: Overview of current understanding, outstanding problems, future research, and explorations significance: Economic Geology, v. 98, p. 1–29.

Heinrich, C.A., Gunther, D., Audedat, A., Ulrich, T., and Frischknecht, R., 1999, Metal fractionation between magmatic brine and vapor, determined by microanalysis of fluid inclusions: Geology, v. 27, p. 755–758.

Holloway, J.R., 1981, Compositions and volumes of supercritical fluids in the earth's crust, *in* Hollister, H.L., and Crawford, M.L., eds., Fluid inclusions: Applications to

petrology: Mineralogical Association of Canada, Short Course Handbook, v. 6, p. 13–38.

Hopeck, J., 2001, Post-Caradocian, pre-Acadian stratigraphy in eastern Maine: Relation of the Aroostook–Matapedia belt to the Miramichi Anticlinorium and the central Maine belt: 93rd Annual Meeting of the New England Intercollegiate Geological Conference, Field Guide Book, p. C4-1–C4-13.

Kerrich, R., 1989, Shear-zone hosted mesothermal gold deposits: A review of geochemical evidence on the sources of fluids and solutes, *in* Bursnall, J.T., ed., Mineralization and shear zone: Geological Association of Canada, Short Course Notes, v. 6, p. 129–197.

Lai, J., and Chi, G., 2007, CO_2-rich fluid inclusions with chalcopyrite daughter mineral from the Fenghuangshan copper-gold deposit, China: Implications for metal transport in vapor: Mineralium Deposita, v. 42, 293–299.

Lang, J.R., and Baker, T., 2001, Intrusion-related gold systems: The present level of understanding: Mineralium Deposita, v. 36, p. 477–489.

Lang, J.R., Baker, T., Hart, C.J., and Mortensen, J.K., 2000, An exploration model for intrusion related gold systems: SEG Newsletter, v. 40, p.1–15.

Le Bas, M.J., Le Maitre, R.W., Streckeisen, A., and Zanettin, B., 1986, A chemical classification of volcanic rocks based on the total alkali-silica diagram: Journal of Petrology, v. 27, p. 745–750.

Leitch, C.H.B., and Lentz, D.R., 1994 , The Gresens approach to mass balance constraints of alteration systems: Methods, pitfalls, examples, *in* Lentz, D.R., ed., Alteration and alteration processes associated with ore-forming systems: Geological Association of Canada, Short Course Notes, v. 11, p. 161–192.

Lentz, D.R., and Gregoire, C., 1995, Petrology and mass-balance constraints on major, trace, and rare-earth-element mobility in porphyry-greisen alteration associated with the epizonal True Hill granite, southwestern New Brunswick, Canada: Journal of Geochemical Exploration, v. 52, p. 303–331.

Loucks, R., and Mavrogenes, J.A., 1999, Gold solubility in supercritical hydrothermal brines measured in synthetic fluid inclusions: Science, v. 284, p. 2159–2163.

Ludwig, K.R., 2001, User's manual for Isoplot/Ex rev. 2.49: A geochronological toolkit for Microsoft Excel: Berkeley Geochronology Centre, Berkeley, Special Publication 1a, 55 p.

McLeod, M.J., and McCutcheon, S.R., 2000, Gold environments in New Brunswick: New Brunswick Department of Natural Resources and Energy, Minerals and Energy Division, Plate 2000-8.

McLeod, M.J., Johnson, S.C., and Ruitenberg, A.A., 1994, Geological map of the southwestern New Brunswick: New Brunswick Department of Natural Resources and Energy, Mineral Resources Map NR-5, scale 1:250 000.

McLeod, M.J., Hoy, D., and Thorne, K., 2008, History of an evolving gold district, southern New Brunswick, Canada: Exploration and Mining Geology, v. 17, no. 1–2, p. 1–12.

NBDNRE, 2000, Bedrock geology of New Brunswick, New Brunswick Department of Natural Resources and Energy, Map NR-1 (2000 Edition), scale 1:500 000.

Pearce, J.A., Harris, N.B.W., and Tindle, A.G., 1984, Trace element discrimination diagrams for the tectonic interpretation of granitic rocks: Journal of Petrology, v. 25, p. 956–983.

Poulsen, K.H., Robert, F., and Dube, B., 2000, Geologic classification of Canadian gold deposits: Geological Survey of Canada Bulletin, v. 540, 106 p.

Rast, N., Lutes, G.G., and St. Peter, C., 1980, The geology and deformation history of the southern part of the Matapedia zone and its relationship to the Miramichi zone and Canterbury basin, *in* Roy, D.C., and Naylor, R.S., eds., A guidebook to the geology of northeastern Maine and neighboring New Brunswick: 72nd Annual Meeting of the New England Intercollegiate Geological Conference, Presque Isle, Maine, p. 191–201.

Renne, P.R., Deino, A.L., Walter, R.C., Turrin, B.D., Swisher, C.C., III, Becker, T.A., Curtis, G.H., Sharp, W.D., and Jaouni, A.R., 1994, Intercalibration of astronomical and radioisotopic time: Geology, v. 22, p. 783–786.

Ridley, J.R., and Diamond, L.W., 2000, Fluid chemistry of orogenic lode gold deposits and implications for genetic models, *in* Hagemann, S.G., and Brown, P.E., eds., Gold in 2000: Reviews in Economic Geology, v. 13, p. 141–162.

Roddick, J.C., 1988, The assessment of errors in $^{40}Ar/^{39}Ar$ dating: Radiogenic age and isotopic studies, report 2: Geological Survey of Canada, Paper 88-2, p. 7–16.

Roddick, J.C., Cliff, R.A., and Rex, D.C., 1980 , The evolution of excess argon in alpine biotites—A $^{40}Ar/^{39}Ar$ analysis: Earth and Planetary Science Letters, v. 48, p. 85–208.

Ruitenberg, A.A., 1994, Metallogeny and lithogeochemistry of the southern Tobique zone, York County, New Brunswick: New Brunswick Department of Natural Resources and Energy, Minerals and Energy Division, Geoscience Report 94-4, 19 p.

Ruitenberg, A.A., Johnson, S.C., and Fyffe, L.R., 1990, Epigenetic gold deposits and their tectonic setting in the New Brunswick Appalachians: CIM Bulletin, v. 83, p. 43–55.

Schmidt Mumm, A., Oberthür, T., Vetter, U., Blenkinsop, T.G., 1997, High CO_2 content of fluid inclusions in gold mineralizations in the Ashanti belt, Ghana: A new category of ore forming fluids: Mineralium Deposita, v. 32, p. 107–118.

Seward, T.M., 1991, The hydrothermal geochemistry of gold, *in* Foster, R.P., ed., Gold metallogeny and Exploration: Blackie, Glasgow and London, p. 37–62.

Sheppard, S.M.F., 1986, Characterization and isotopic variations in natural water, *in* Valley, J.W., Taylor, H.P.Jr., and O'Neil, J.R., eds., Stable isotopes in high-temperature geological processes: Reviews in Mineralogy, v. 16, p. 165–183.

Soave, G., 1972 , Equilibrium constants from a modified Redlich-Kwong equation of state: Chemical Engineering Science, v. 27, p. 1197–1203.

Stern, R.A., 1997, The GSC Sensitive High Resolution Ion Microprobe (SHRIMP): Analytical techniques of zircon U–Th–Pb age determinations and performance evaluation: Radiogenic age and isotopic studies, report 10: Geological Survey of Canada, Current Research 1997-F, p. 1–31.

Stern, R.A., and Amelin, Y., 2003, Assessment of errors in SIMS zircon U–Pb geochronology using a natural zircon standard and NIST SRM 610 glass: Chemical Geology, v. 197, p. 111–146.

Taylor, B.E., 1986, Magmatic volatiles: Isotopic variation of C, H, and S, *in* Valley, J.W., Taylor, H.P. Jr., and O'Neil, J.R., eds., Stable isotopes in high-temperature geological processes: Reviews in Mineralogy, v. 16, p. 185–225.

Thompson, J.F.H., and Newberry, R.J., 2000, Gold deposits related to reduced granitic intrusions, *in* Hagemann, S.G., and Brown, P.E., eds., Gold in 2000: Reviews in Economic Geology, v. 13, p. 377–400.

Valley, J.W., 1986, Stable isotope geochemistry of metamorphic rocks, in Valley, J.W., Taylor, H.P. Jr., and O'Neil, J.R., eds., Stable isotopes in high-temperature geological processes: Reviews in Mineralogy, v. 16, p. 45–489.

van Staal, C., 1994, Brunswick subduction complex in the Canadian Appalachians: Record of the Late Ordovician to Late Silurian collision between Laurentia and the Gander margin of Avalon: Tectonics, v. 13, p. 946–962.

Villeneuve, M.E., and MacIntyre, D.G, 1997, Laser $^{40}Ar/^{39}Ar$ ages of the Babine porphyries and Newman Volcanics, Fulton Lake map area, west-central British Columbia: Radiogenic age and isotopic studies, report 10: Geological Survey of Canada, Current Research 1997-F, p.131–139.

Villeneuve, M.E., Sandeman, H.A., and Davis, W.J., 2000, A method for the intercalibration of U–Th–Pb and $^{40}Ar/^{39}Ar$ ages in the Phanerozoic: Geochimica et Cosmochimica Acta, v. 64, p. 4017–4030.

Watters, S.E., 1998, Report on geological-structural mapping, Poplar Mountain grid: Poplar Mountain project of Freewest Resources Canada Inc., Fosterville, New Brunswick: Freewest Resources Canada Inc., internal Report, 34 p.

Watters, S.E., and Chi, G., 2002, Detailed bedrock geology of the Poplar Mountain gold deposit (part of NTS 21 G/13), York County, New Brunswick: New Brunswick Department of Natural Resources and Energy, Mineral, Policy and Planning Division, Plate 2002-58.

Whalen, J.B., Rogers, N., van Staal, C.R., Longstaffe, F.J., Jenner, G.A., and Winchester, J.A., 1998, Geochemical and isotopic (Nd, O) data from Ordovician felsic plutonic and volcanic rocks of the Miramichi Highlands: Petrogenetic and metallogenic implications for the Bathurst mining camp: Canadian Journal of Earth Sciences, v. 35, p. 237–252.

Williams, H., 1995, Temporal and spatial divisions, *in* Williams, H., ed., Geology of the Appalachian-Caledonian orogen in Canada and Greenland: Geological Survey of Canada, Geology of Canada, No. 6, p. 21–44.

Winchester, J.A., and Floyd, P.A., 1977, Geochemical discrimination of different magma series and their differentiation products using immobile elements: Chemical Geology, v. 20, p. 325–343.

Yang, X., Lentz, D.R., and Chi, G., 2002, Petrochemistry of Lake George granodiorite stock and related Au mineralization, York County, New Brunswick: Geological Survey of Canada, Current Research, 2002-D, 10 p.

Zheng, Y.-F., 1999, Oxygen isotope fractionation in carbonate and sulfate minerals: Geochemical Journal, v. 33, p. 109–126.

Appendix

Analytical Methods of U–Pb and $^{40}Ar/^{39}Ar$ Isotopic Dating

U–Pb Analyses: U–Pb ion probe data were acquired using the Geological Survey of Canada Sensitive High Resolution Ion Microprobe (SHRIMP II). SHRIMP analytical methods are provided in detail in Stern (1997), with standards and U–Pb calibration methods following Stern and Amelin (2003). The sample was crushed in a jaw crusher and ground in a disk mill; the heavy mineral fraction was separated using a Wilfley Table and heavy liquid separation. Zircons were mounted and polished along with grains of the GSC zircon standard (BR266: $^{206}Pb/^{238}U$ age = 559 Ma) in a 2.5 cm epoxy puck (GSC #240). Back-scattered electron and cathodoluminescence images were made utilizing a Cambridge Instruments scanning electron microscope to fully characterize the internal structures of the grains and aid in-beam positioning. Mount surfaces were evaporatively coated with 10 nm of high-purity Au. Analyses were conducted using an $^{16}O-$ primary beam, projected onto the zircons at 10 kV. The sputtered area used for analysis was ca. 15 μm in diameter with a beam current of ca. 3.5 nA. The count rates of ten isotopes of Zr^+, U^+, Th^+, and Pb^+ in zircon were sequentially measured (6 scans) with a single electron multiplier and a pulse counting system with deadtime of 24 ns. Off-line data processing was accomplished using customized in-house software. The 1σ external errors of $^{206}Pb/^{238}U$ ratios reported in Table 2 incorporate a ±1.0% error in calibrating the standard zircon (see Stern and Amelin, 2003). No fractionation correction was applied to the Pb-isotope data; common Pb correction utilized the measured $^{204}Pb/^{206}Pb$ and compositions modeled after Cumming and Richards (1975). Isoplot v. 2.49 (Ludwig, 2001) was used to generate concordia plots and calculate weighted mean ages. Ages reported in text are quoted at 2σ level of uncertainty.

$^{40}Ar/^{39}Ar$ Analyses: Sericite was separated by standard mineral separation techniques and was loaded into aluminum foil packets along with a single grain of Fish Canyon Tuff Sanidine (FCT-SAN) to act as flux monitor (apparent age = 28.03 ± 0.1 Ma; Renne et al., 1994). The sample packets were arranged radially inside an aluminum can. The samples were then irradiated for 12 hours at the research reactor of McMaster University in a fast neutron flux of

approximately 3×10^{16} neutrons/cm^2. Laser $^{40}Ar/^{39}Ar$ step-heating analysis was carried out at the Geological Survey of Canada laboratories in Ottawa, Ontario. Irradiated samples were split into several aliquots and loaded into individual 1.5 mm-diameter holes in a copper planchet. The planchet was then placed in the extraction line and the system evacuated. Heating of individual sample aliquots in steps of increasing temperature was achieved using a Merchantek MIR10 10W CO_2 laser equipped with a 2 mm $\times$ 2 mm flat-field lens. The released Ar gas was cleaned over getters for ten minutes, and then analyzed using the secondary electron multiplier system of a VG3600 gas source mass spectrometer; details of data collection protocols can be found in Villeneuve and MacIntyre (1997), and Villeneuve et al. (2000). Neutron flux gradients throughout the sample canister were evaluated by analyzing the sanidine flux monitors included with each sample packet and interpolating a linear fit against calculated J-factor and sample position. The error on individual J-factor values is conservatively estimated at ±0.6% (2σ). Because the error associated with the J-factor is systematic and not related to individual analyses, correction for this uncertainty is not applied until calculation of dates from isotopic correlation diagrams (Roddick, 1988). No evidence for excess ^{40}Ar was observed in any of the samples and, therefore, all regressions are assumed to pass through the $^{40}Ar/^{36}Ar$ value for atmospheric air (295.5). All errors are quoted at 2σ level of uncertainty.